Journal Name

Dynamic Article Links ►

Cite this: DOI: 10.1039/c0xx00000x

www.rsc.org/xxxxxx

ARTICLE TYPE

Cyanamide Route to Calcium-Manganese Oxide Foams for Water Oxidation

Elham Baktash[a], Ivelina Zaharieva*[b], Marc Schröder[c], Caren Goebel[a], Holger Dau*[b] and Arne Thomas*[a]

[a] *Technische Universität Berlin, Department of Chemistry, Hardenbergstr. 40, 10623 Berlin, Germany Fax: +49 30 314 29271; Tel.: +49 30 314 25118; E-mail: arne.thomas@tu-berlin.de*

[b] *Freie Universität Berlin, Department of Physics, Arnimallee 14, 14195 Berlin, Germany; Fax: +49 30 838 56299; Tel: +49 30 838 53581; E-mail: ivelina.zaharieva@fu-berlin.de; holger.dau@fu-berlin.de,*

[c] *Technische Universität Berlin, Department of Chemistry, Straße des 17. Juni 124, 10623 Berlin*

In nature, photosynthetic water oxidation is efficiently catalysed at a protein-bound μ-oxido Mn_4Ca cluster. This cluster consists of earth abundant, non-toxic elements and serves as a paragon for development of synthetic catalysts. In this work we developed porous calcium-manganese oxides with a unique foam-like nanostructure prepared via a facile and robust synthetic route using cyanamide as porogen. A series of such oxide foams annealed at different temperatures was characterized by TEM, SEM, XRD, N_2 physisorption, and X-ray absorption spectroscopy (XAS) in order to correlate crystallinity, atomic structure, surface area and oxidation state of the materials with catalytic activity. Some of the resulting Ca-Mn oxides show high activity as catalysts for water oxidation in presence of cerium(IV) ammonium nitrate as a non-oxo transfer oxidant. An amorphous calcium-manganese-oxide foam with 130 $m^2.g^{-1}$ surface area and Mn oxidation state of +3.6 was identified to be most active; its activity is superior to previously reported Ca-Mn oxides. At the atomic level, this material shares structural motifs with the biological paragon as revealed by dual-edge XAS at the Mn and Ca *K*-edge. Rather than nanostructure and surface area, the atomic structure of the Ca-Mn oxide and the extent of structural order appear to be crucial determinants of catalytic activity. Fully disordered low-valent Mn materials as well as high-valent but crystalline Mn-Ca oxides are unreactive. Highly disordered variants of layered manganese oxide with Ca and water molecules interfacing layer fragments are most reactive.

Introduction

Dioxygen formation by catalytic water oxidation is an essential half reaction for important processes such as water splitting or artificial photosynthesis.[1] Beside noble metals (RuO_2[2], IrO_2[3],...), transition metal oxides, such as cobalt[4], manganese[5, 6, 7] and nickel oxides[8] have been shown to be active and robust catalysts for this reaction. For example MnO_2[9] and Mn_2O_3[5] catalyse water oxidation in presence of different oxidizing agents. Following these pioneering works different manganese oxides have been prepared which show promising activity towards water oxidation in presence of non-oxo transfer oxidants, for example λ-MnO_2[10], α-MnO_2 nanowires and nanotubes, β-MnO_2 nanowires[11], nano-sized α-Mn_2O_3[12] and amorphous manganese oxides.[13]

Often metal oxides with a high level of amorphicity at both the nanostructural and atomic level showed high activity but the insight in structure-reactivity relations has remained insufficient. On the other hand, well-ordered (diffracting) manganese hydroxides and oxides showed catalytic activity in water oxidation, but only at comparatively low level.[14-17] Inspired by the biological catalysts bound to the proteins of photosystem II, the photosynthetic $Mn_4Ca(\mu\text{-}O)_n$ cluster,[18] calcium-manganese oxides have been also studied as water oxidation catalysts. Indeed, it has been recently shown that incorporation of calcium ions can improve the catalytic activity of synthetic Mn oxides pronouncedly, but only for formation of amorphous Ca-Mn oxides.[19, 20]

Increasing the surface area of heterogeneous catalysts, either by forming smaller particles or by creating pores, is a practical pathway to increase the catalytic efficiency of solid materials. For the generation of porous materials most often templating approaches are applied. For example the inorganic phase can be formed in presence of an organic porogen, which afterwards is removed leaving behind more or less defined pores in the inorganic matrix. We have recently presented a pathway to prepare highly porous silicas in a one-step approach by adding cyanamide to a silica precursor solution and subsequent gelation and heat treatment of this mixture. Heat treatment of cyanamide yield, over several polycondensation steps, a polymeric carbon nitride, which acted as hard template to create the porosity in the silica.[21] Herein we used a comparable approach, namely mixing Ca-Mn oxide precursors with cyanamide and additional heat treatment. However, here the organic porogen decomposed already at lower temperatures leaving behind a porous, foam-like Ca-Mn oxide. Different cyanamide/metal ratios were applied and the resulting Ca-Mn oxide foams were calcined at different temperatures, to gain a series of oxides, which were tested as catalysts for water oxidation. The structure of the formed materials was investigated by X-ray absorption spectroscopy at

the Mn and Ca *K*-edge, powder XRD and (HR)TEM and the results suggests that in this case the surface area is not the decisive factor that determines the catalytic activity.

Experimental Section

Synthesis of $CaMn_2O_x$-A-B

0.687 g of $Mn(NO_3)_2.4H_2O$ and 0.32 g of $Ca(NO_3)_2.4H_2O$ were dissolved in 2 ml distilled water. To this solution an aqueous solution of different amounts of cyanamide (0.8, 4.0 and 8.0 g, conc. 1.0 g/ml, "A" denotes the amount of cyanamide used) was added and the resulting mixture was stirred for 3 h in air (pH=1). The final solution was poured into a Petri dish and heated at 100°C for 30 h. The resulting brown-grey solid is scratched from the Petri dish and calcined in ambient conditions at different temperatures (T_{calc}= 300°C, 400°C, 550°C, 700°C, 1000°C, "B" denotes the applied calcination temperature). A heating ramp with the rate of 3°C/min was used until the final temperature was reached and then the samples were heated for 4h at this temperature.

Two reference materials were also prepared, one without cyanamide (A=0), the other without calcium.

Characterization

X-ray diffraction (XRD) patterns were measured in reflection mode on a Bruker D8 Advance X-ray diffractometer using $CuK\alpha_1$ irradiation (λ=0.154 nm). IR spectra were measured on a Varian 1000 FTIR spectrometer using an ATR technique.

The microstructure (morphology, crystallinity, particle size, chemical composition) of the samples were studied by electron microscopy at the Department of Electron Microscopy ZELMI, TU Berlin. Transmission Electron Microscopy (TEM) measurements were operated by a FEI Tecnai G2 20 S-TWIN transmission electron microscope equipped with a LaB_6-source at 200 kV acceleration voltages. For TEM-investigations a small amount of the sample powder was placed on a TEM-grid (carbon film on 300 mesh Cu-grid, Plano GmbH, Germany) and was sputtered with carbon. EDX-analysis were carried out with an EDAX r-TEM SUTW Detector (Si (Li)-detector). Images were recorded with a GATAN MS794 P CCD-camera.

For Scanning Electrone Microscope (SEM) analysis a small amount of the sample powder was placed on a conducting carbon pad (Plano GmbH, Germany) and sputtered with a thin carbon layer. The investigations were performed by means of a JXA-8530F microprobe (JEOL GmbH, Germany) equipped with a field emission source. Qualitative chemical analysis and beam scan mapping were carried out by 20 kV acceleration voltage with integrated energy dispersive X-ray spectroscopy using a SDD detector.

Specific surface area of samples were determined at liquid-nitrogen temperature (-196 °C) with an Autosorb-1 Instrument. The sample was degassed at 150 °C overnight before measurement. The Brunauer-Emmett-Teller (BET) surface area was calculated by multiple-point (five-point) measurement in the relative pressure range of 0.05-0.30.

Thermogravimetric analysis (TGA) measurements were carried out on a STA6000 from Perkin-Elmer in ambient condition at a temperature range of 30-1000 °C with the heating rate of 10 °C/min. The amount of metal in the samples was determined by inductively coupled plasma atomic emission spectroscopy, using an ICP-OES 517 (Varian Inc., USA).

X-ray absorption spectra (XANES/EXAFS) were collected at the BESSY synchrotron radiation source operated by the Helmholtz-Zentrum Berlin. The measurements were acquired at the KMC-1 bending-magnet beamline at 20 K in a cryostat (Oxford-Danfysik) with a liquid-helium flow system. The oxide powder samples were diluted by thorough mixing with boron nitride (BN) powder (Sigma Aldrich) to the ratio 1:10. The measurements at the manganese *K*-edge were performed in transmission mode with an ionization chamber and the spectra at the Ca *K*-edge were detected in fluorescence mode using 13-element energy-resolving Ge detector (Canberra). Further details are given in ref.[22].

Oxygen evolution was measured using a Clark-type oxygen electrode system (Strathkelvin, 1302 oxygen electrode and 782 oxygen meter). An air saturated water solution and zero-oxygen (sodium sulfite in water) solution were used for the calibration of the electrode. In a typical run oxygen evolution was detected with electrode under stirring in an anaerobic solution of oxides in presence of 0.5 M $(NH_4)_2Ce(NO_3)_6$ (See SI). An Agilent 7890A gas chromatograph was used to determine the oxygen content in the headspace of the reactor. The GC was equipped with a carboxen-1000 column and a thermal conductivity detector (TCD). The carrier gas was argon (30 mL min^{-1}). Calibration was done with oxygen gas mixture of defined concentrations (1, 10 vol%).

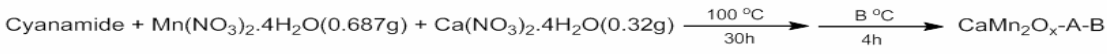

Scheme 1. Synthetic route of $CaMn_2O_x$-A-B with different amount of porogen and various calcination temperatures (A= 0.8, 4 and 8 g, B= 300, 400, 550, 700, 1000 ºC).

Results and discussion

For the preparation of porous calcium manganese oxides, aqueous solutions of calcium and manganese (II) nitrates were mixed with cyanamide. After removal of water (by evaporation at 100 ºC), the resulting solid mixtures were heated to different temperatures (Scheme 1). Two series of calcium manganese oxides have been prepared using either different amounts of cyanamide or different calcination temperatures. Depending on the amount of used cyanamide and calcination temperature, samples are denoted $CaMn_2O_x$-A-B (A is the amount of cyanamide in gram and B the calcination temperature in ºC).

Similar to previous works of Kurz [19] and Shilov[9] we used simple Mn^{2+} and Ca^{2+} salts as precursors. However in our synthetic route we do not add an oxidant (MnO_4^-). Instead oxidation of Mn is induced by heating the Mn-Ca mixture in presence of oxygen. When no cyanamide is added (e.g. $CaMn_2O_x$-0-550), a non-porous mixture of crystalline phases is

formed, which just showed very low catalytic activity for water oxidation. However, the addition of cyanamide yield materials with increased surface area and strongly affects the atomic structure of the formed oxides, which eventually results in the formation of highly active catalysts (see below).

It has been described that upon thermal treatment, cyanamide transforms via several condensation steps into dicyandiamide, melamine, melem and finally into melon, a polymeric carbon nitride.[23, 24] Such polymeric carbon nitrides are just formed at temperatures as high as 550 ºC and have recently gained increasing interest for their application as photocatalysts.[23] Decomposition of such carbon nitrides finally occur at around 650 ºC. However in the present system no formation of a polymeric carbon nitride was observed at temperatures above 300 ºC. Indeed TGA measurements (Figure S1) and elemental analysis showed that only in the sample prepared at 300 ºC ($CaMn_2O_x$-0.8-300) a considerable amount of organic moieties can be found, while already at 400 ºC ($CaMn_2O_x$-0.8-400) only minor contributions of carbon and nitrogen residues are detectable (N%:0.8, C%: 1.9) suggesting that the formed CaMn oxide accelerates decomposition of the carbon nitride precursors drastically. TGA measurement of the oxides heated to lower temperatures (300°C/400°C) also show considerable weight losses in the temperature range of 30-400 ºC, which is explained by the loss of water weakly bound to the oxide layers. Further weight loss in the range of 400 °C to 1000 °C can be explained by phase transition with oxygen release e.g. by reduction of manganese from Mn^{4+} to Mn^{3+} and finally Mn^{2+}.[25]

In the infrared (IR) spectra (Figure S2), broad bands around 3300 cm^{-1} and 1640 cm^{-1} are assignable to O-H stretching and H-O-H bending mode vibrations of water. They are especially pronounced in $CaMn_2O_x$-0.8-400, confirming the presence of sizeable amounts of water. The vibrational modes of the MnO_6 units expand over the 700-400 cm^{-1} region, as expected for Mn oxides.[26] ICP-OES was carried out to determine the calcium and manganese content of the oxides and showed that the Ca:Mn ratio in calcium manganese oxides remained unchanged during the preparation process (Ca:Mn~ 1:2) (Table S1).

Table 1 Characterization of oxides prepared at different calcination temperatures.

Catalyst	S_{BET} [a]	Oxygen evolution rate [b]	Crystal Size [c]	Oxidation state	Parent phase
$CaMn_2O_x$-0.8-300	0.2	0.011	Amorphous	2.1[f]	Mn^{2+} and Ca^{2+} in amorphous organic matrix
$CaMn_2O_x$-0.8-400	130	3.0/0.42[g]	Amorphous, <5[d]	3.6[f]	Layer-type $CaMn_2^{III/IV}$ oxide, fully amorphous
$CaMn_2O_x$-0.8-550	62	0.62	5-18	3.7[f]	similar $Ca_2Mn_3O_8$
$CaMn_2O_x$-0.8-700	19	0.082	17-53	3.8[f]	$Ca_2Mn_3O_8$
$CaMn_2O_x$-0.8-1000	3.3	0.018	40-93	3[e]	$CaMn_2O_4$ (marokite)
Mn_2O_3-0.8-550	36	0.10	15-38	3[e]	Mn_2O_3

Table 2 Characterization of oxides prepared with different amount of porogen.

Catalyst	S_{BET} [a]	Oxygen evolution rate [b]	Crystal Size [c]	Oxidation state	Resolved parent phase(s)
$CaMn_2O_x$-8-550	46	0.14	11-39	-	$Ca_2Mn_3O_8$
$CaMn_2O_x$-4-550	51	0.22	7-27	-	$Ca_2Mn_3O_8$
$CaMn_2O_x$-0.8-550	62	0.62	5-18	3.7[f]	$Ca_2Mn_3O_8$
$CaMn_2O_x$-0-550	3.9	0.029	16-66	3.9[e]	mixture of oxide phases[h]

[a]Surface area of oxides ($m^2.g^{-1}$), [b] oxygen evolution rate ($mmol_{O2}.mol_{Mn}^{-1}.s^{-1}$) in presence of $[Ce^{4+}]$= 0.5 M, [c]Crystal size (nm) calculated based on Scherrer equation of XRD peaks, [d] Crystal or particle size as estimated from (HR)TEM image, [e]Oxidation state as deduced from XRD results (Figure S3-5), [f]Oxidation state based on XANES data, [g]Oxygen evolution rate ($mmol_{O2}.mol_{Mn}^{-1}.s^{-1}$) in presence of $[Ce^{4+}]$= 0.5 M resulted from long-term measurement by gas chromatography (Figure S15, Table S4)), [h]XRD reflections were assigned to MnO_2, Mn_2O_3, Ca_2MnO_4, and CaO; alternative assignments are not excluded..

X-ray powder diffraction (XRD) was used to identify the formed oxide phases. Figure 1a shows the XRD patterns of samples produced with constant amount of cyanamide but different calcination temperatures ($CaMn_2O_x$-0.8-B). The oxide heated to 300 °C is completely XRD amorphous. By heating the sample to 400 ºC, a broad peak of low intensity at 2θ=29.4° may be

observable, which cannot be easily assigned. Partial crystallisation (lowered amorphicity) of the samples is observed for oxides heated to 550°C. At 700 °C, the XRD peaks become more intense and can be finally assigned to a layered $Ca_2Mn_3O_8$ structure (Figure S3).[27, 28] Further heating to 1000 °C yielded a complete phase change from $Ca_2Mn_3O_8$ to $CaMn_2O_4$ (Figure S4).

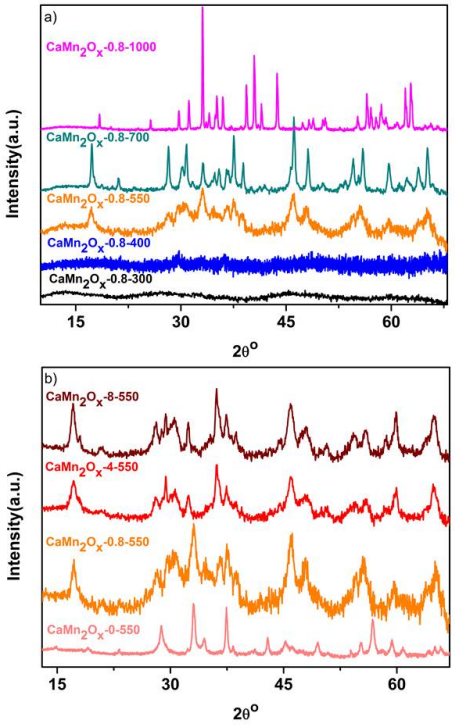

Figure 1. XRD patterns of a) $CaMn_2O_x$-0.8-B calcined at different temperatures and b) $CaMn_2O_x$-A-550 prepared with different amount of cyanamide porogen.

XRD patterns of the oxides heated to 550°C and prepared with different amount of cyanamide are shown in Figure 1b ($CaMn_2O_x$-A-550). All patterns point toward the presence of $Ca_2Mn_3O_8$, however the broad peaks again point toward a high level of amorphicity.

The broad XRD peaks are explainable either by very small crystallites (see 'crystal size' in Tables 1 & 2) or by structural disorder (amorphicity) at the atomic level resulting, e.g., from a high number of defect sites or lack of a well-defined unit cell. The XRD pattern generally reflects the pair distribution function (PDF) of the atoms in the diffracting material; for ideal XRD data, the PDF can be obtained directly from the XRD pattern by appropriate Fourier transformation. For non-crystalline samples of limited long-range order, broad reflections may be observable which are assignable to the 'parent structure' of a crystalline material. Accordingly we suggest that the temperature increase from 400°C via 550°C to 700°C (Fig. 1a) results in increasing similarity of the material to the same parent structure, namely $Ca_2Mn_3O_8$. This suggestion is supported by the EXAFS data presented further below. (Here and in the following, we use the term 'parent structure' to denote a crystalline material which contains a set of structural motifs also found in the amorphous materials. In the amorphous material however, mixed oxidation states, the presence of water molecules, and other factors result in a low degree of order such that the structural motifs of the parent structure become less prominent.)

As visible in Fig. 1b, more intense but still broadened peaks for the layered $Ca_2Mn_3O_8$ are observed with increasing amount of cyanamide. Alternatively, when no cyanamide was added ($CaMn_2O_x$-0-550) the formation of $Ca_2Mn_3O_8$ is not observed anymore. Instead reflections assignable to different Mn and Ca oxide phases or parent structures are observed (Table 2, Figure S5). XRD analysis thus shows that the addition of cyanamide to the precursor mixture not only introduces porosity (see below) but is also responsible for a phase change of the Ca-Mn oxides during heat treatment.

Calcium manganese oxides have been prepared without addition of cyanamide.[19] These oxides showed long range metal-metal interaction at 400°C and even at 60°C which indicates the formation of pre-ordered structures already at low temperature.[29]In the herein described protocol, cyanamide condensation forms an organic framework below 400°C and metal ions are at this stage most likely coordinated to the building blocks of the framework (Tri-s-triazines, melamine, etc.). This results in their spatial separation and therefore inhibition of formation of any specific oxide phase. In fact, no long-range metal-metal interaction can be found in the composites until the calcination temperature approaches 550°C (see below). By heating the sample to 400°C the organic network decomposes and a calcium manganese oxide with highly disordered nature is formed, proven by XRD and XAS. Thus the formation of different phases of CaMn oxide with and without cyanamide might be explained by the very different temperatures at which first formation of long-range order and eventually crystallization occurs.

Transmission electron microscopy (TEM) was used to reveal the structure of the materials (Figure 2 and Figure S6-8). $CaMn_2O_x$-0.8-300 shows no distinct features, but a rather intimate mixture between Ca-Mn oxide and carbon nitride precursors at this temperature. As mentioned before, between 300 °C and 400 °C the organic phase disappears forming gaseous decomposition products and nearly pure Ca-Mn oxide remains. Indeed $CaMn_2O_x$-0.8-400 shows a foam-like structure as it is typically observed in polymers when gaseous products are formed during polymerization. The foam structure can be also observed by SEM measurements (Figure 2f). When heated to 550 °C, the porous structure becomes denser, with an average decrease in pore size that may be due to the reduced amorphicity and water loss of the material resulting in structural contraction. At 700 °C the foam or porous structure completely disappears and instead larger particles are observed. EDS-mapping images (Figure S9-S11) prove a homogenous distribution of calcium, manganese and oxygen within all the samples calcinated at temperatures above 300 °C, rendering a phase separation, e.g., between one calcium oxide and one or more manganese oxides unlikely. While in the XRD no reflections are observed for $CaMn_2O_x$-0.8-400, (HR)TEM images analyzed by Fast Fourier-Transformation reveal a diffuse diffraction ring and weak diffraction reflexes corresponding to d-values of $Ca_2Mn_3O_8$ phase (Figure S7). The d-value of 2.9 Å is in agreement with the

EXAFS results revealing a prominent Mn-Mn distance of 2.87 Å. (HR)TEM images of the samples $CaMn_2O_x$-0.8-550 and $CaMn_2O_x$-0.8-700 confirm the XRD results; they suggest the presence of a layered $Ca_2Mn_3O_8$ (parent) structure (Figure S8). This structure can be described as vacancy-containing sheets of edge-sharing MnO_6 octahedra which are interconnected by Ca^{2+} ions[27, 28] (Figure S12).

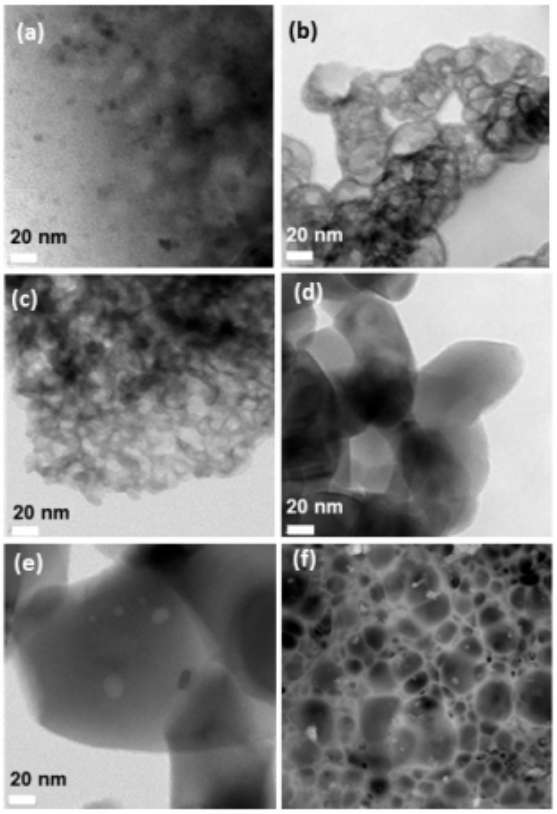

Figure 2. (a-e)TEM images of calcium manganese oxide samples which were calcined at a) 300 °C, b) 400 °C, c) 550 °C, d) 700 °C, e) 1000 °C, f) SEM images of $CaMn_2O_x$-0.8-400.

Nitrogen sorption experiments showed that the herein presented preparation method resulted in oxides with increased surface areas (Tables 1, 2). While from the pure Ca and Mn salts, Ca-Mn oxides (e.g. $CaMn_2O_x$-0-550) with lower outer surface areas (~4 $m^2.g^{-1}$) are observed, addition of cynanamide yields surface areas up to 130 $m^2.g^{-1}$ for $CaMn_2O_x$-0.8-400 and 62 $m^2.g^{-1}$ for $CaMn_2O_x$-0.8-550. The chosen amount of 0.8 g cyanamide seems to be optimal for creating the porous structure as a further increase does not yield higher surface areas. A higher amount of template of course yields thinner pore walls in the replica. Thus, when a certain cyanamide/metal ratio is reached, structural collapse and a decrease in the overall surface area can be observed. As confirmed by electron microscopy measurements, the porosity of the samples collapsed when prepared with higher amounts of cyanamide (Figure S6) or at higher temperatures, i.e. at 700 °C and 1000°C (Figure 2) and consequently lower surface areas and porosities are observed.

We note that the achieved surface area of 130 $m^2.g^{-1}$ for $CaMn_2O_x$-0.8-400 is still lower than the surface area of previously reported MnCa oxides[19] with surface areas of 205 $m^2.g^{-1}$ or 303 $m^2.g^{-1}$. In spite of the lower surface areas, the MnCa oxides described herein excel by clearly higher oxygen evolution activity (Table S2), as discussed in the following.

Oxygen evolution

Water-oxidation experiments were carried out in presence of a non-oxygen transfer oxidizing agent, cerium ammonium nitrate, to investigate the catalytic activity of the oxides (Figure 3, S13 and Tables 1, 2 and S2,3). Ce^{4+} is a single electron oxidant with a high oxidation potential (Ce^{4+}/Ce^{3+}, E_0 ~ +1.4V vs. NHE) suitable for water oxidation. It has been proven by ^{18}O-labelling experiments that reactions in which Ce^{4+} act as oxidant and manganese oxides as catalysts are ''real'' water-oxidation processes as bulk water provides both oxygen atoms of the produced O_2.[13, 30] Our experiments were conducted in 2 ml deoxygenated aqueous solutions containing the Ca-Mn oxide and cerium ammonium nitrate. A Clark-type electrode was used for detection of dissolved oxygen produced in these solutions. Figure 3 shows the dissolved oxygen content in the solutions at room temperature. All compounds are active for water-oxidation while $CaMn_2O_x$-0.8-400 is by far the most active one showing a rate of 3 $mmolO_2.molMn^{-1}.s^{-1}$. Furthermore, long-term oxygen evolution and stability test with gas chromatography showed that $CaMn_2O_x$-0.8-400 is active for extended time periods in harsh conditions (60 h, pH ~1) and can produce oxygen in a second and third run at almost the same rate (Figure S14, S15, Table S4). The long term measurements showed lower initial oxygen evolution rates compared to the ones measured by the Clark electrode (Table 1, S4) which might be due to the different experimental conditions and setups. The oxygen evolution rate seem also to decrease with time, which however can be explained by the consumption of the oxidant (Ce(IV)). Indeed addition of fresh oxidant after 60 h showed that the catalyst remains active, even after long time periods. The same result is seen when a lower amount of catalyst was used (Fig S14b and c). Still it should be mentioned that also in this experiments a decrease in the oxygen evolution rate is found, so that also some deactivation of the catalysts over time has to be assumed.

Partially crystalline $CaMn_2O_x$-0.8-550, which is the second best catalyst, showed clearly lower rate of 0.62 $mmolO_2.molMn^{-1}.s^{-1}$. The crystalline $CaMn_2O_x$-0.8-700 is nearly inactive (oxygen evolution rate of 0.082 $mmolO_2.molMn^{-1}.s^{-1}$). Two samples were prepared as references, $CaMn_2O_x$-0-550 without cyanamide and Mn_2O_3-0.8-550 without calcium, in order to study the role of these two components in the catalytic activity of resulting oxides. The catalytic activity of Mn_2O_3-0.8-550 and $CaMn_2O_x$-0-550 is 6 and 21 times lower, respectively, compared to $CaMn_2O_x$-0.8-550. In both cases the resulting oxides had completely different atomic structure. In the absence of Ca^{2+}, Mn_2O_3 is formed, while in absence of cyanamide a mixture of several crystalline phases is obtained (Fig. S5).

In recent works it has been suggested that layered Mn oxide phases have the highest activity in catalytic water oxidation.[20, 22, 29, 31, 32] Moreover, it has been shown that the Ca^{2+} ion is an important cofactor in biological oxygen evolution,[33] it may

control charge balance and oxidation potential of the Mn_4Ca complex.[34] The Ca^{2+} ion also may act as a Lewis acid to activate water molecules for nucleophilic attack on the electrophilic oxygen atom of Mn-oxyl intermediate.[35, 36] Likewise, in the layered oxides incorporation of Ca^{2+} ion seems to be crucial to increase their activity for water oxidation.[19, 20, 29, 37] In our case, indeed Mn_2O_3-0.8-550 showed a much lower catalytic activity than $CaMn_2O_x$-0.8-550.

The manganese oxidation state in the synthesized oxides may be among the crucial determinants of catalytic activity. The average oxidation states were estimated by means of XANES (X-ray absorption near-edge structure) analysis and are presented in Table 1 and 2. In the oxide with the highest water-oxidation activity ($CaMn_2O_x$-0.8-400), manganese shows an average oxidation state of +3.6. It was shown for oxides used as catalysts[38] or electrocatalysts[6, 17] that the performances of materials containing Mn^{3+} was superior compared to the ones with pure Mn^{4+}, which suggests that presence of Mn^{3+} is essential for having an active catalyst. On the other hand, oxides containing

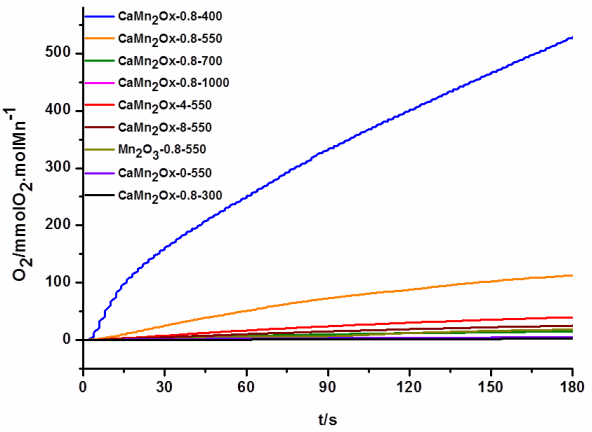

Figure 3. Oxygen evolution in 0.5 M aqueous Ce^{4+} solution.

Mn^{3+} only (e.g. Mn_2O_3-0.8-550 in our study) are also poor catalysts[11, 12], supporting that the presence of both Mn^{3+} and Mn^{4+} in a suitable ratio enhance the catalytic activity.[29]

We note that interpretation of the average oxidation state detected for the various oxides of the present investigation cannot be approached in a fully unambiguous way. An average oxidation state of +3.6 might not result from a mixed-valent $Mn^{3+/4+}$ oxide but from a mixture of a Mn^{3+} oxide, e.g. Mn_2O_3 or $CaMn_2O_4$, and a Mn^{4+} oxide, e.g. β-Mn_2O or $Ca_2Mn_3O_8$. Indeed, a mixture of microcrystalline phases of various oxides may be present in the inactive, cyanamide-free $CaMn_2O$-0-550 (see XRD data in Fig. S5a). Yet in the oxides of high water oxidation activity ($CaMn_2O_x$-0.8-400/550), the XRD and EXAFS data is best explained in terms of a single phase of a mixed-valent $Mn^{3+/4+}$ oxide.

Manganese oxidation states

The X-ray absorption near-edge spectra (XANES) recorded at the Mn *K*-edge, allowed us to estimate the mean oxidation state of manganese in the samples annealed at different temperatures (Table 1, Figure S16). As evident from the energy shift of the position of the main absorption edge,[39] above 300 °C the mean formal oxidation state of Mn increases from 2 to above 3.5, indicating that most of the initial Mn^{2+} is oxidized to Mn^{4+} although some low-valence Mn ions are still present. At 1000 °C however, Mn^{4+} is reduced to Mn^{3+}, the typical Mn oxidation state found in marokite ($CaMn_2O_4$).[40] Similar Mn-oxidation state changes in mixed CaMn oxides upon annealing were observed before.[29] To follow the associated structural changes in the CaMn oxides and to identify the basic structural motifs in the amorphous catalytically active materials, we used extended range dual-edge EXAFS spectroscopy, recording spectra at both Mn and Ca *K*-edges (Figure 4, Figure S17).

Information on atomic structure from EXAFS

X-ray absorption spectra[39, 41] were collected at the *K*-edges of both, manganese (~6550 eV) and calcium (~4040 eV). The X-ray absorption near-edge structure (XANES; Figure S16) of the Mn *K*-edge facilitated the above estimates of the mean manganese oxidation states. The Ca-XANES (Figure S16) indicates significant changes in the calcium ligand environment but cannot be easily interpreted in terms of specific structural changes.

Within about 1000 eV above the respective X-ray edge, the extended X-ray absorption fine-structure (EXAFS) was detected. The EXAFS carries information on distances between the X-ray absorbing atom (Mn or Ca) and atoms of the first, second, and higher coordination spheres. The latter atoms are denoted as backscatters as they facilitate backscattering of the photoelectron wave created at the absorber atom. In the Fourier-transformed EXAFS spectra (Figure 4), each peak corresponds to an absorber-backscatter distance, which is by 0.3-0.4 Å longer than the indicated reduced distance.[39 41]

The first peak of the Fourier-transformed Mn-EXAFS at reduced distances around 1.5 Å is assignable to the oxygen atoms in the first manganese coordination sphere at distances of 1.9 Å or larger. *The second peak* at reduced distance of 2.4 Å corresponds to a Mn-Mn distance of 2.87 Å (as revealed by EXAFS simulations) and is assignable to a pair of di-μ-oxo bridged Mn ions (edge-sharing MnO_6 octahedra). *The third peak* of Mn-only oxides (e.g. Mn_2O_3-0.8-550) mostly is assignable to pairs of mono-μ-oxo bridged Mn ions with typical distances close to 3.4 Å. In the MnCa oxides however, there are contributions to the third EXAFS peak resulting from calcium ions connected by several bridging oxygens to manganese ions. *The two long-distance peaks* at reduced distance of about 5.3 and 4.6 Å are assignable to backscattering by manganese ions in the fourth and fifth coordination sphere of the X-ray absorbing manganese (see structural motif indicated in Figure 4); the presence of these two peaks is indicative of long-range order (crystallinity or low level of amorphicity).

Visual inspection of the Mn-EXAFS spectra before (Figure S17) or after Fourier-transformation (Figure 4) reveals that for increasing the temperature from 400 via 550 to 700 °C, the long-range order increases (increased long-distance peaks, Figure 4; increased EXAFS amplitudes at higher *k*-values, Figure S17). However, the basic shape of the spectra remains the same suggesting that the increase in calcination temperature from 400 to 700 °C causes lowered amorphicity (higher crystallinity) without changing the central structural motifs present in the first

and second coordination sphere of the Mn ions. For calcination temperatures below 400 °C, no metal-metal distance are resolved suggesting that the metal ions are not interconnected by bridging oxides but merely coordinated to water molecules and cyanamide-derived ligands.

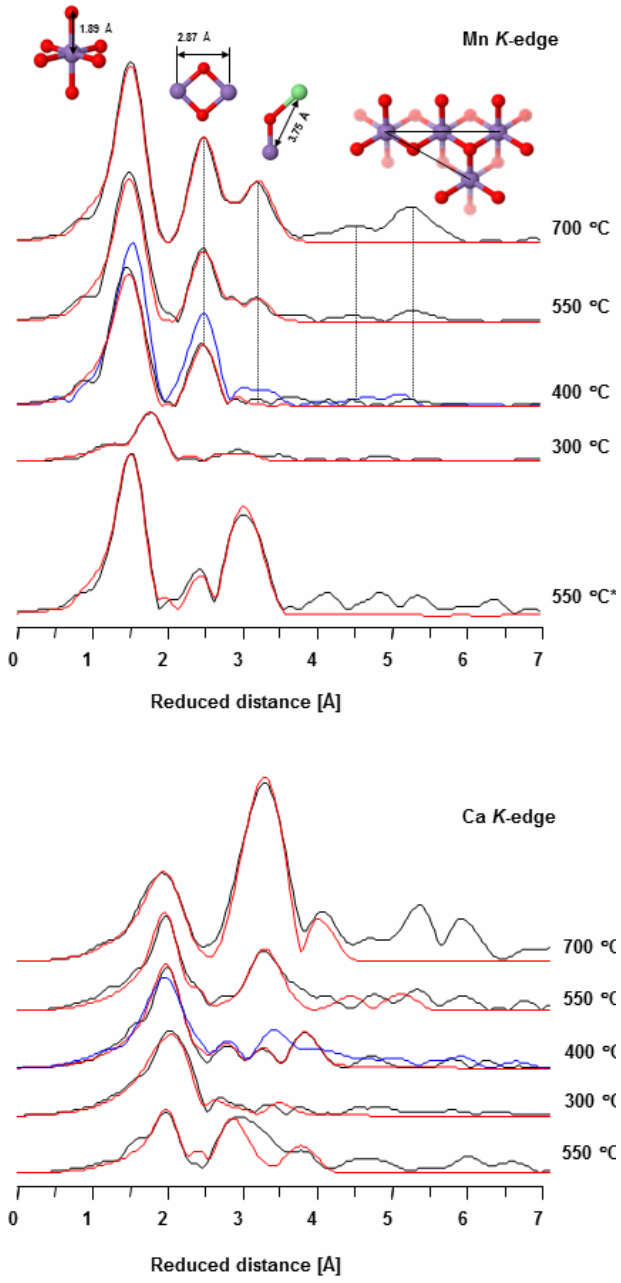

Figure 4. Fourier-transformed EXAFS spectra measured at the Mn *K*-edge (top panel) and at the Ca *K*-edge (bottom panel). We note that the indicated 'reduced distances' are by 0.3-0.4 Å shorter than the atom-atom distances as obtained by EXAFS simulations at high precision. Black lines, experiment; red lines simulations; blue line, spectra of the catalytically active $CaMn^{IV}_{1.6}Mn^{III}_{0.4}O_{4.5}(OH)_{0.5}$ oxide investigated in ref29. The asterisk (550 °C*) indicates the sample prepared without cyanamide. The structural motifs corresponding to each of the main peaks are schematically depicted (Mn in magenta, Ca in green, O in red).

In clear contrast, the Ca-EXAFS differs pronouncedly between oxides calcined at 400 °C and 700 °C (Figure 4, Figure S17) indicating a pronounced change in the ligand environment of the X-ray absorbing calcium ions. This can be explained as follows. Most likely the calcium ions are located in the space between layers of edge-sharing MnO_6 octahedra. In the highly ordered and largely dehydrated oxide created by calcination at 700 °C and resembling crystalline $Ca_2Mn_3O_8$ closely, the majority of calcium ions may directly interconnect layers of edge-sharing MnO_6 octahedra (see Figure S12, left panel). However in the water-rich oxide obtained by moderate calcination at 400 °C, the calcium ions are coordinated to several water molecules of the interlayer space.

Precise atom-atom distances were obtained by simulating simultaneously the Mn-EXAFS and the Ca-EXAFS using a joint-fit approach described before.[29] The simulated spectra are shown in Figure S17 and Figure 4; simulation parameters, are given in Table S5 and Figure S18. For the $CaMn_2O_x$-0.8-700 oxide, the EXAFS simulation results confirm the prevalence of the $Ca_2Mn_3O_8$ structure indicated by the XRD, even though the Ca:Mn stoichiometries differ. The distances between µ-oxo bridged Mn-Mn and Mn-Ca pairs as determined by the EXAFS simulations agree well with the corresponding distances of the crystallographic model.[27, 28] Two Mn-Ca distances of 3.3 Å and 3.7 Å are resolved by EXAFS simulations. They are assignable to $CaMn_3(\mu\text{-}O)_4$ structures resembling distorted cubanes (3.3 Å) and to a motif of Ca ions capping missing layer-building Mn ions (3.7 Å, see Figure 5). The characteristic 2.88 Å distance for di-µ-oxo connected Mn ions of layered oxides[42] is well resolved, as well as Ca-Ca distances of $Ca_2Mn_3O_8$.

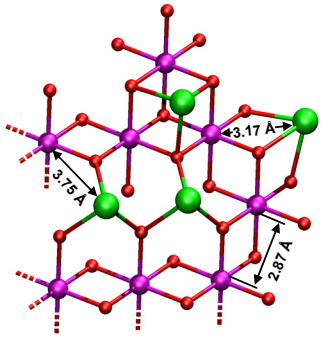

Figure 5. Structural model of a fragment from catalytically active CaMn oxide. The presence of distances close to 3.8 and 3.2 Å is suggested by the EXAFS data collected at the Ca *K*-edge, but is not resolved (3.8 Å) or not well resolved (3.2 Å) in the Mn-EXAFS simulations (see Table S5). The first coordination sphere of calcium is complemented either by µ-oxo bridges to manganese ions or by water molecules. The color code is the same as in Fig. 4.

Both XRD and XAS strongly suggest the presence of $Ca_2Mn_3O_8$ in $CaMn_2O_x$-0.8-700. There are two possible explanations for the mismatch in the Ca:Mn stoichiometry (1:2 in the synthesized oxide versus 2:3 in $Ca_2Mn_3O_8$): (a) Aside from $Ca_2Mn_3O_8$ crystallites, a largely amorphous CaMn oxide with low Ca content is present in $CaMn_2O_x$-0.8-700. (b) The $Ca_2Mn_3O_8$ structure may be viewed as layers of edge-sharing MnO_6 octahedra with Mn-vacancies capped by calcium ions;

removal of capping calcium ions and filling of the corresponding Mn-vacancies could result in a major change in the Ca:Mn stoichiometry, without modification of other unit cell parameters.

The latter explanation (that is, (b)) is in good agreement with the EXAFS results, but also (a) cannot be ruled out definitively. The EDS mapping supports (b) because two distinct phases differing in the Ca:Mn stoichiometry are not detectable. However, the spatial resolution of the presented EDS-mapping data might be insufficient to resolve different phases in neighbouring small crystallites. Whether (b) is in conflict with the XRD powder diffraction data remains an open question. Conclusive XRD analysis of amorphous materials or crystallites with imperfect crystalline order requires extensive simulations which are beyond the scope of the present work.

Distances similar to the ones found in $CaMn_2O_x$-0.8-700 are also found in $CaMn_2O_x$-0.8-550 (Table S5). However the coordination numbers for the metal-metal distances are lower suggesting prevalence of a clearly less ordered structure, that is, a clearly higher level of amorphicity in $CaMn_2O_x$-0.8-550.

At 400 °C calcination, the coordination numbers of the 2.9 Å Mn-Mn distance are even lower (lower amplitude of second Fourier peak). All Mn-Mn distances exceeding 3 Å result in small contributions to the EXAFS only (see Figure 4) indicating an especially high level of amorphicity. Consequently the Mn-EXAFS simulation results of Table S5 which relate to Mn-Mn/Ca distances exceeding 3 Å are of low significance. It is likely that the Mn-Ca motifs with characteristic Mn-Ca distances of 3.4 Å (cubane) and 3.7 Å (Ca capping Mn-layer-vacancy) are also present in $CaMn_2O_x$-0.8-400, but clearly less frequently than in the oxides calcined at 550 and 700°C. Noteworthily, the amorphicity of $CaMn_2O_x$-0.8-400 is even higher than observed for oxides previously synthesized in the absence of cyanamide (blue lines in Figure 4).[19]

In summary, calcination at temperatures higher than 300 °C induces formation of high-valent $Mn^{III/IV}$ oxides which consist of vacancy-rich layers of edge-sharing MnO_6 octahedra. These oxides may be considered as being relatives of layered oxides with one layer (birnessite) or two layers (buserite) of water molecules and cations interconnecting MnO_2 layers.[43] For calcinations at 400 °C, the MnCa oxide is highly disordered, providing an especially high number of both protonatable (and potentially reactive) μ_2-O(H) bridges and terminal water-coordination sites.[44]

This may explain the especially high water-oxidation activity of $CaMn_2O_x$-0.8-400, which exceeds the activity of better ordered MnCa oxides previously synthesized in the absence of cyanamide[19]. At higher calcinations temperatures (550 and 700°C), the structure becomes increasingly well-ordered and approaches the 'parent structure' of crystalline $Ca_2Mn_3O_8$ closely.

Without addition of cyanamide but using otherwise the same synthesis protocol, an entirely different structure is formed, which is dominated by mono-μ-oxo bridging between manganese ions, This structure exhibits higher crystallinity and shows similarities to the β-MnO_2 crystalline phase (1 x 1 tunnel Mn oxides),[45] but not to the layered birnessite-like oxides.[46, 47]

Conclusions

We reported a simple, robust and easily reproducible synthetic protocol resulting in highly active mixed MnCa oxide catalyst for water oxidation. CaMn oxides have been prepared by adding cyanamide to the Ca and Mn precursor salts and subsequent thermal treatment. Cyanamide or more probably one of its condensation and decomposition products acts as porogen and foam-like porous CaMn oxides are observed. Analysis of crystal and atomic structure of the resulting CaMn oxides show that besides pore formation and surface area, cyanamide strongly influences also the prevalent Mn oxidation state, the atomic structure, and the level of amorphicity. It is generally assumed that all these factors can influence the catalytic activity of CaMn oxides for water oxidation, while the surface area seem to be no decisive factor determining the water oxidation activity in amorphous materials (Figure S19). In other words the presented results indicate that the catalytic reaction may take place also at the active centres formed in the bulk phase of the amorphous materials. At the atomic level, a structure containing poorly ordered layered fragments build from di-μ-oxo connected Mn ions (in mixed oxidation states of +3 and +4) and coordinatively non-saturated oxygens in bridging positions establish the catalytic properties of the synthetic oxides. Incorporation of Ca^{2+} in the structure presumable contributes to the achieved high catalytic rates.

Acknowledgement

Financial support from the Cluster of Excellence ''Unifying Concepts in Catalysis'' (EXL 31411) and the project "Nachhaltige Chemie (Sustainable Chemistry)" funded by the senate of Berlin is gratefully acknowledged. We thank Dr. P. Chernev, Katharina Klingan and J. Heidkamp for their essential contributions in the XAS experiments. We acknowledge support by the BESSY synchrotron (Berlin) operated by the Helmholtz-Zentrum Berlin (HZB), specifically the excellent technical support by M. Mertin and Dr. F. Schäfers. The authors express their gratitude to Jörg Nissen from the Department of Electron Microscopy ZELMI, TU Berlin for the SEM measurements.

References

1. H. Dau, C. Limberg, T. Reier, M. Risch, S. Roggan and P. Strasser, *ChemCatChem*, 2010, **2**, 724-761.
2. C. Minero, E. Lorenzi, E. Pramauro and E. Pelizzetti, *Inorg. Chim. Acta,* 1984, **91**, 301-305.
3. F. A. Frame, T. K. Townsend, R. L. Chamousis, E. M. Sabio, T. Dittrich, N. D. Browning and F. E. Osterloh, *J. Am. Chem. Soc*., 2011, **133**, 7264-7267.
4. M. W. Kanan and D. G. Nocera, *Science*, 2008, **321**, 1072-1075.
5. A. Harriman, I. J. Pickering, J. M. Thomas and P. A. Christensen, *J. Chem. Soc., Faraday Trans. 1 F*, 1988, **84**, 2795-2806.
6. M. Morita, C. Iwakura and H. Tamura, *Electrochim. Acta*, 1977, **22**, 325-328.

7. K. Mette, A. Bergmann, J.-P. Tessonnier, M. Hävecker, L. Yao, T. Ressler, R. Schlögl, P. Strasser and M. Behrens, *ChemCatChem*, **4**, 851-862.
8. M. DincÄƒ, Y. Surendranath and D. G. Nocera, *PNAS*, 2010, **107**, 10337-10341.
9. V. Y. Shafirovich and A. E. Shilov, *Kinet. Katal.*, 1979, **20**, 1156-1162.
10. R. Brimblecombe, A. Koo, G. C. Dismukes, G. F. Swiegers and L. Spiccia, *J. Am. Chem. Soc.*, 2012, **132**, 2892-2894.
11. V. B. R. Boppana and F. Jiao, *Chem. Commun.*, 2011, **47**, 8973-8975.
12. M. M. Najafpour, F. Rahimi, M. Amini, S. Nayeri and M. Bagherzadeh, *J. Chem. Soc., Dalton Trans.*, 2012, **41**, 11026-11031.
13. A. Iyer, J. Del-Pilar, C. K. King ondu, E. Kissel, H. F. Garces, H. Huang, A. M. El-Sawy, P. K. Dutta and S. L. Suib, *J. Phys. Chem. C.*, 2012, **116**, 6474-6483.
14. F. Cheng, J. Shen, B. Peng, Y. Pan, Z. Tao and J. Chen, *Nat. Chem.*, 2011, **3**, 79-84.
15. Y. Gorlin and T. F. Jaramillo, *J. Am. Chem. Soc.*, 2010, **132**, 13612-13614.
16. N. P. Luneva, V. Y. Shafirovich and A. E. Shilov, *J. Mol. Catal. A: Chem.*, 1989, **52**, 49-62.
17. S. Trasatti, *Journal of J. Electroanal. Chem. Interfacial Electrochem.*, 1980, **111**, 125-131.
18. H. Dau, I. Zaharieva and M. Haumann, *Curr. Opin. Chem. Biol.*, 2012, **16**, 3-10.
19. M. M. Najafpour, T. Ehrenberg, M. Wiechen and P. Kurz, *Angew. Chem., Int. Ed.* , 2010, **49**, 2233-2237.
20. M. Wiechen, I. Zaharieva, H. Dau and P. Kurz, *Chem. Sci.*, 2012, **3**, 2330-2339.
21. K. Kailasam, J. D. Epping, A. Thomas, S. Losse and H. Junge, *Energy Environ. Sci.*, 2011, **4**, 4668-4674.
22. I. Zaharieva, P. Chernev, M. Risch, K. Klingan, M. Kohlhoff, A. Fischer and H. Dau, *Energy Environ. Sci.*, 2012, **5**, 7081-7089.
23. A. Thomas, A. Fischer, F. Goettmann, M. Antonietti, J.-O. Muller, R. Schlogl and J. M. Carlsson, *J. Mater. Chem.*, 2008, **18**, 4893-4908.
24. B. V. Lotsch and W. Schnick, *Chem. Eur. J.*, 2007, **13**, 4956-4968.
25. N. N. Greenwood and A. Earnshaw, *Chemistry of the Elements*, Butterworth-Heinemann, Oxford, 1997.
26. C. M. Julien, M. Massot and C. Poinsignon, *Spectrochim. Acta, Part A*, 2004, **60**, 689-700.
27. G. B. Ansell, M. A. Modrick, J. M. Longo, K. R. Poeppeimeler and H. S. Horowitz, *Acta Crystallogr., Sect. B: Struct. Sci*, 1982, **38**, 1795-1797.
28. T. R. White, W. S. Glaunsinger, H. S. Horowitz and J. M. Longo, *J. Solid State Chem.*, 1979, **29**, 205-214.
29. I. Zaharieva, M. M. Najafpour, M. Wiechen, M. Haumann, P. Kurz and H. Dau, , *Energy Environ. Sci.*, 2011, **4**, 2400-2408.
30. D. Shevela, S. Koroidov, M. M. Najafpour, J. Messinger and P. Kurz, *Chem. Eur. J.*, 2011, **17**, 5415-5423.
31. R. K. Hocking, R. Brimblecombe, L.-Y. Chang, A. Singh, M. H. Cheah, C. Glover, W. H. Casey and L. Spiccia, *Nat. Chem.*, 2011, **3**, 461-466.
32. B. A. Pinaud, Z. Chen, D. N. Abram and T. F. Jaramillo, *J. Phys. Chem. C.*, 2011, **115**, 11830-11838.
33. H. Dau and M. Haumann, *Coord. Chem. Rev.*, 2008, **252**, 273-295.
34. E. Y. Tsui, R. AU - Tran, J. AU - Yano and T. AU - Agapie, *Nat. Chem.*, 2013.
35. J. Limburg, V. A. Szalai and G. W. Brudvig, *J. Chem. Soc., Dalton Trans.*, 1999, **0**, 1353-1362.
36. M. J. B. V. L. Pecoraro, M. T. Caudle, W.-Y. Hsieh and N. A. Law, *Pure Appl. Chem.*, 1998, **70**, 925-929.
37. M. M. Najafpour, *J. Chem. Soc., Dalton Trans.*, 2011, **40**, 3793-3795.
38. F. Jiao and H. Frei, *Chem. Commun.*, 2010, **46**, 2920-2922.
39. H. Dau, P. Liebisch and M. Haumann, *Anal. Bioanal.Chem.*, 2003, **376**, 562-583.
40. S. Zouari, L. Ranno, A. Cheikh-Rouhou, O. Isnard, M. Pernet, P. Wolfers and P. Strobel, *J. Alloys Compd.*, 2003, **353**, 5-11.
41. J. E. Penner-Hahn, *Coord. Chem. Rev.*, 1999, **190-192**, 1101-1123.
42. M. Villalobos, B. Lanson, A. Manceau, B. Toner and G. Sposito, *Am. Mineral.*, 2006, **91**, 489–502.
43. J. E. Post, *PNAS*, 1999, **96**, 3447-3454.
44. H. Dau, C. Limberg, T. Reier, M. Risch, S. Roggan and P. Strasser, *ChemCatChem*, **2**, 724-761.
45. R. W. G. Wyckoff, *Crystal Structures*, Interscience Publishers, New York, 1963.
46. B. M. Tebo, J. R. Bargar, B. G. Clement, G. J. Dick, K. J. Murray, D. Parker, R. Verity and S. M. Webb, *Annu. Rev. Earth Planet. Sci.*, 2004, **32**, 287-328.
47. T. G. Spiro, J. R. Bargar, G. Sposito and B. M. Tebo, *Acc. Chem. Res.*, 2010, **43**, 2-9.

Supporting Information

Cyanamide Route to Calcium-Manganese Oxide Foams for Water Oxidation

Elham Baktash[a], Ivelina Zaharieva*[b], Marc Schröder[c], Caren Goebel[a], Holger Dau*[b] and Arne Thomas*[a]

[a] *Technische Universität Berlin, Department of Chemistry, Hardenbergstr. 40, 10623 Berlin, Germany Fax: +49 30 314 29271; Tel.: +49 30 314 25118; E-mail: arne.thomas@tu-berlin.de*

[b] *Freie Universität Berlin, Department of Physics, Arnimallee 14, 14195 Berlin, Germany; Fax: +49 30 838 56299; Tel: +49 30 838 53581; E-mail: zahariev@zedat.fu-berlin.de; holger.dau@fu-berlin.de*

[c] *Technische Universität Berlin, Department of Chemistry, Straße des 17. Juni 124, 10623 Berlin*

The Supporting information contains:

1. Details on oxygen evolution experiments

2. The following additional figures and tables;

Figure S1. TGA curves for the thermal decomposition of calcium manganese oxides.

Figure S2. IR spectra of CaMn oxides calcined at 400 °C, 550 °C, 700 °C and 1000 °C.

TableS1 and S2. ICP data of samples $CaMn_2O_x$-0.8-550, $CaMn_2O_x$-4-550 and $CaMn_2O_x$-8-550

Figure S3. XRD patterns of oxides $CaMn_2O_x$-0.8-550, $CaMn_2O_x$-0.8-700 and $Ca_2Mn_3O_8$.

Figure S4. XRD patterns of $CaMn_2O_x$-0.8-1000 and $CaMn_2O_4$.

Figure S5. XRD patterns of a) $CaMn_2O_x$-0-550 and b) Mn_2O_3-0.8-550.

Figure S6. TEM images of a) $CaMn_2O_x$-0.8-550, b) $CaMn_2O_x$-4-550, c) $CaMn_2O_x$-8-550 and (HR)TEM images of d) $CaMn_2O_x$-0.8-550, e) $CaMn_2O_x$-4-550, f) $CaMn_2O_x$-8-550.

Figure S7. (HR)TEM images and FFTs of $CaMn_2O_x$-0.8-400 which shows d-values corresponding to $Ca_2Mn_3O_8$ (hkl=-311).

Figure S8. TEM images and FFTs of a,b) $CaMn_2O_x$-0.8-550 which shows d-values corresponding to $Ca_2Mn_3O_8$ (hkl=-111) and c,d) $CaMn_2O_x$-0.8-700 with d-values corresponding to $Ca_2Mn_3O_8$ (hkl=111).

Figure S9. SEM image and EDS-mapping of $CaMn_2O_x$-0.8-400.

Figure S10. SEM image and EDS-mapping images of o $CaMn_2O_x$-0.8-550.

Figure S11. SEM image and EDS-mapping images of $CaMn_2O_x$-0.8-700.

Figure S12. Structure of $Ca_2Mn_3O_8$. A – side view where the MnO_6 layers and the Ca ions between them are visible. B – top view illustrating the two binding positions of Ca: on the top of Mn vacancies (3.84 Å Mn-Ca distance) and in a cubane motif (3.17 Å Mn-Ca distance). Mn atoms are shown in magenta, Ca in green, and O in red.

Table S3. Oxygen evolution data from refs.[1,2] and this investigation).

Figure S13. Oxygen evolution results for the reaction of CaMn oxides suspended in 0.5 M Ce^{4+} aqueous solution.

Table S4: Amount of dissolved oxides (mg/ml) in solution (0.5M Ce(IV)).

Figure S14: Long term oxygen evolution test (100mg catalyst in 38ml of Ce(IV) solution, $CaMn_2O_x$-0.8-400, Ce(IV)= 0.5M). Oxygen evolution was measured by gas chromatography. The result shows that although the oxygen evolution rate has been decreased after first 20h but it is producing oxygen until the end of reaction time and the catalyst remains active for longer time either by addition of fresh oxidant or using less amount of catalyst.

Figure S15: Recycling experiments using $CaMn_2O_x$-0.8-400 = 2.8 mg/ml, Ce(IV)= 0.5M.

Table S5: Details of catalytic test experiments by gas chromatography.The data show small change in T.O.F. even with different amount of catalyst or using the same one for second and third run (T.O.F. has been calculated based on the oxygen amount(mmol)produced in the first 30min of the reaction and divided by the amount of manganese content of the catalyst(mol).

Figure S16. XANES spectra measured at the Mn *K*-edge (top) and the Ca *K*-edge (bottom) from the CaMn material before annealing (100 °C) and after annealing for 4h at different temperatures. Insets: comparison of the XANES spectra from CaMn oxide with and without cyanamide, annealed at 550 °C.

Figure S17. k^3 weighted EXAFS spectra measured at the Mn *K*-edge (top) and the Ca *K*-edge (bottom) from the CaMn material before annealing (100 °C) and after annealing for 4h at different temperatures. Black: experimental curves, red - simulations. The simulation parameters are shown in Table S1.

Table S6. EXAFS simulation parameters.

Figure S18. Coordination numbers deduced from the simulations, as shown also in Table S1. A: measurements at the Mn *K*-edge, B: at the Ca *K*-edge.

Figure S19. Rate of O_2-formation (R_{O2}) per surface area (A). If O_2-rate were proportional to the surface area, R_{O2}/A should be independent on the surface (A). Instead, a decreased activity per surface area by two orders of magnitude is observed meaning that the surface area is not a crucial determinant of the rate of catalysis (see dotted line drawn to guide the eye) (refs.[1,2] and this investigation).

1. *Details on the oxygen evolution experiments*

For a typical catalytic experiment, oxides were suspended in water in a Schlenk tube. Then these solutions were made anaerobic by nitrogen purging ($[O_2] < 1$ µmol/l) and the oxygen level was monitored by a Clark electrode. After an equilibriation time of 2 min, an anaerobic solution of Ce(IV) was injected into the tube using a nitrogen-purged syringe. The dissolved oxygen produced during the reaction was monitored by a Clark electrode. The initial oxygen evolution rates as shown in Table 1 and 2 were determined by a linear fit of the Clark cell data of the first three minutes and divided by the amount of the overall manganese content in the oxide suspended in the 2 ml reaction solution (Table S2). In pursuing these experiments, it was been considered that the Clark electrode can detect dissolved oxygen reliably only below the O_2-saturation point of water (258 µmol/l, T=25°C).

The long term experiments were carried out as follows: Millipore water was sonicated under reduced pressure for 1 h. Millipore water was sonicated under reduced pressure for 1 h. Afterwards the water solution was flushed with argon for 1 h to remove all oxygen. The catalyst and the magnetic stir bar were placed into the reaction chamber and the reactor was closed. Subsequent oxygen was removed by applying vacuum and flushing the reactor with argon. This procedure was repeated 3 times. The reaction mixture, consisting of Ce(IV) in water (0.5 M), with a total volume of 38 mL, was prepared in an oxygen evacuated flask. Then the reaction solution was added to the reaction chamber under reverse argon flow using a dosing valve. After closing the dosing valve, thermostat, magnetic stirrer, and the online measurement software were started. For the second injection the reactor has been opened under Argon, flushed with this gas, and then closed after the injection. The data after oxidant addition was added to the first graph assuming that flushing the reactor with Ar removed all oxygen produced in the first step (See ref 3 for more details about setup).[1]

The TOF has been calculated based on the oxygen amount (in mmol) produced in the first 30 min of the reaction and divided by the amount of manganese of the catalyst (in mol).

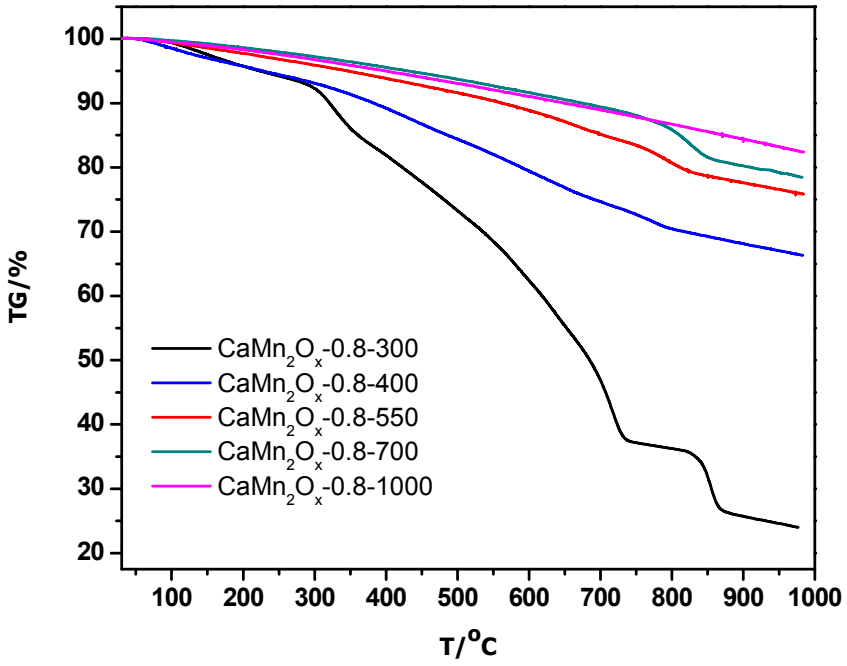

Figure S1. TGA curves for the thermal decomposition of calcium manganese oxides (measurements were carried out on a STA6000 from Perkin-Elmer in ambient condition at a temperature range of 30-1000 °C with the heating rate of 10 °C/min.)

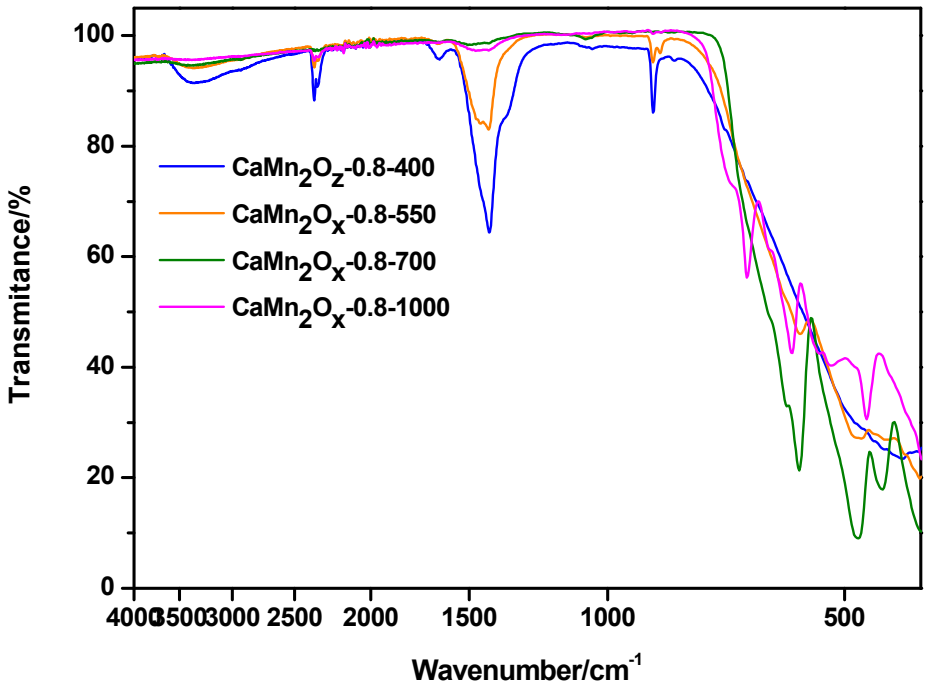

Figure S2. IR spectra of CaMn oxides calcined at 400 °C, 550 °C, 700 °C and 1000 °C.

Table S1and S2. ICP data of $CaMn_2O_x$-0.8-550, $CaMn_2O_x$-4-550, and $CaMn_2O_x$-8-550

Sample	Ca:Mn
$CaMn_2O_x$-0.8-300	1:1.80
$CaMn_2O_x$-0.8-400	1:1.20
$CaMn_2O_x$-0.8-550	1:2.04
$CaMn_2O_x$-4-550	1:2.05
$CaMn_2O_x$-8-550	1:2.10
$CaMn_2O_x$-0.8-700	1:1.38

Sample	%Mn(w)	%Ca(w)
$CaMn_2O_x$-0.8-300	27.64	11.27
$CaMn_2O_x$-0.8-400	40.71	14.75
$CaMn_2O_x$-0.8-550	50.40	18
$CaMn_2O_x$-4-550	52.35	18.63
$CaMn_2O_x$-8-550	54.3	18.77
$CaMn_2O_x$-0.8-700	41.82	21.95

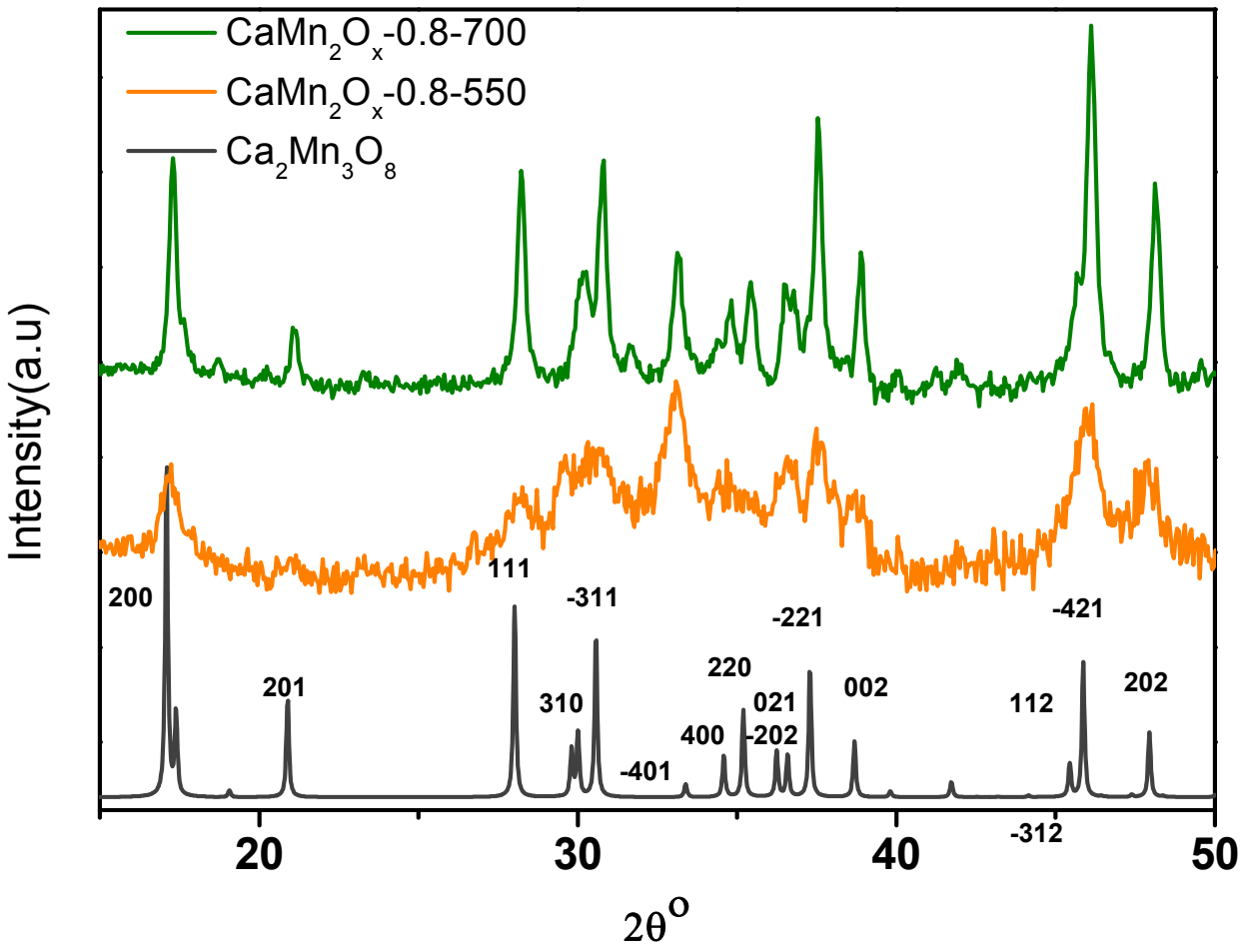

Figure S3. XRD patterns of oxides $CaMn_2O_x$-0.8-550, $CaMn_2O_x$-0.8-700 and $Ca_2Mn_3O_8$.

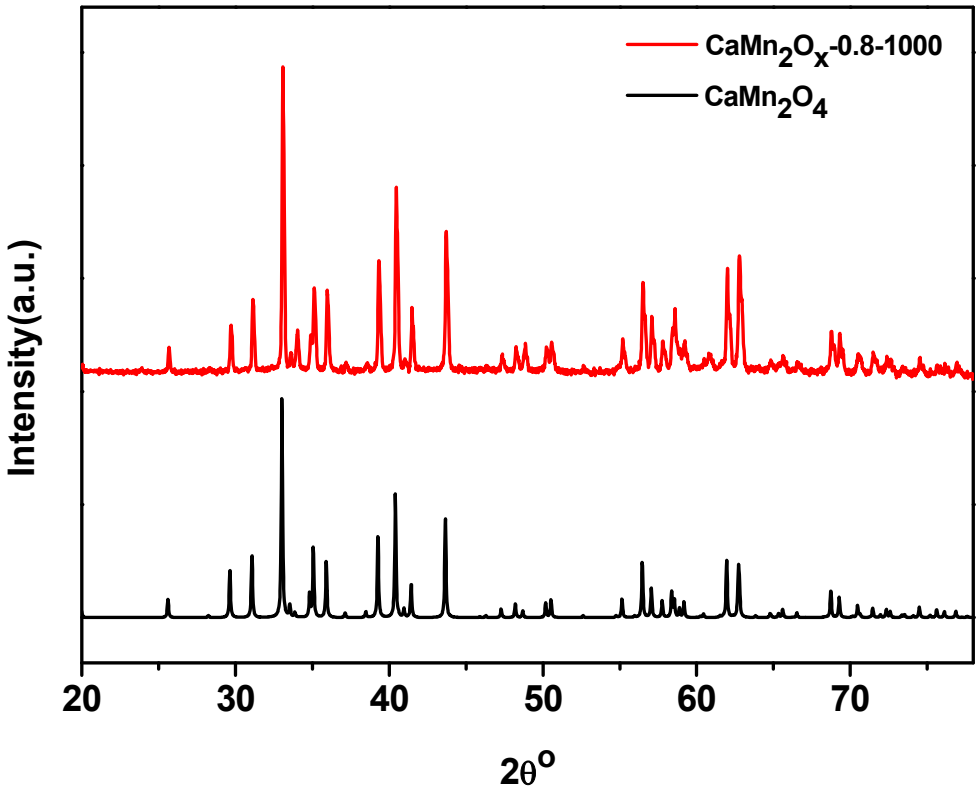

Figure S4. XRD patterns of $CaMn_2O_x$-0.8-1000 and $CaMn_2O_4$, for comparison.

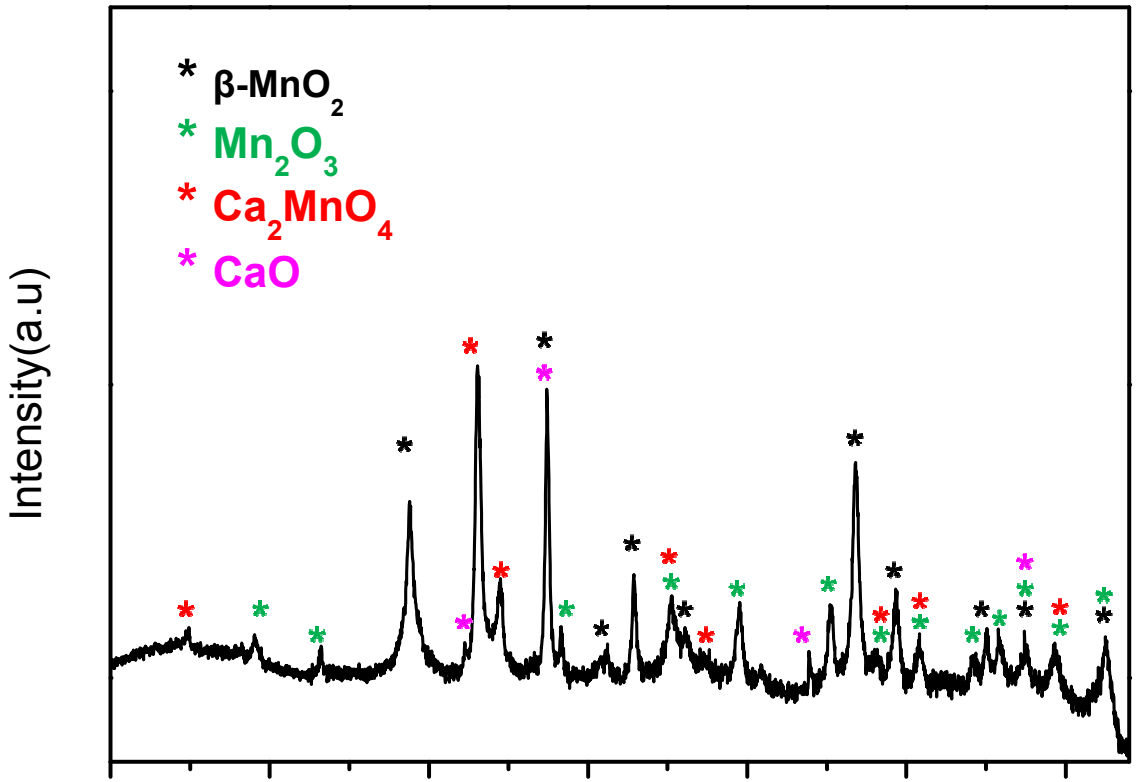

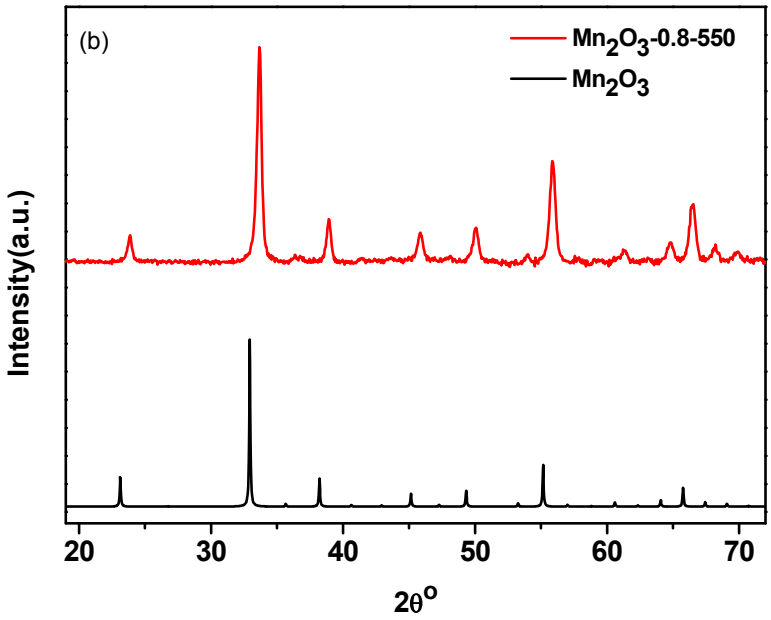

Figure S5. XRD patterns of a) $CaMn_2O_x$-0-550 and b) Mn_2O_3-0.8-550. In a), the stars label reflections that are found in crystalline calcium and manganese oxides at similar diffraction angles. We note that this assignment does not necessarily mean that there is a phase separation involving four distinct oxide phases. For amorphous materials, the XRD pattern reflects the pair distribution function (as obtained by appropriate Fourier-transformation of the XRD pattern); a single amorphous phase may be characterized by reflections of several parent structures. In b), the reflection pattern of Mn_2O_3 is shown for comparison.

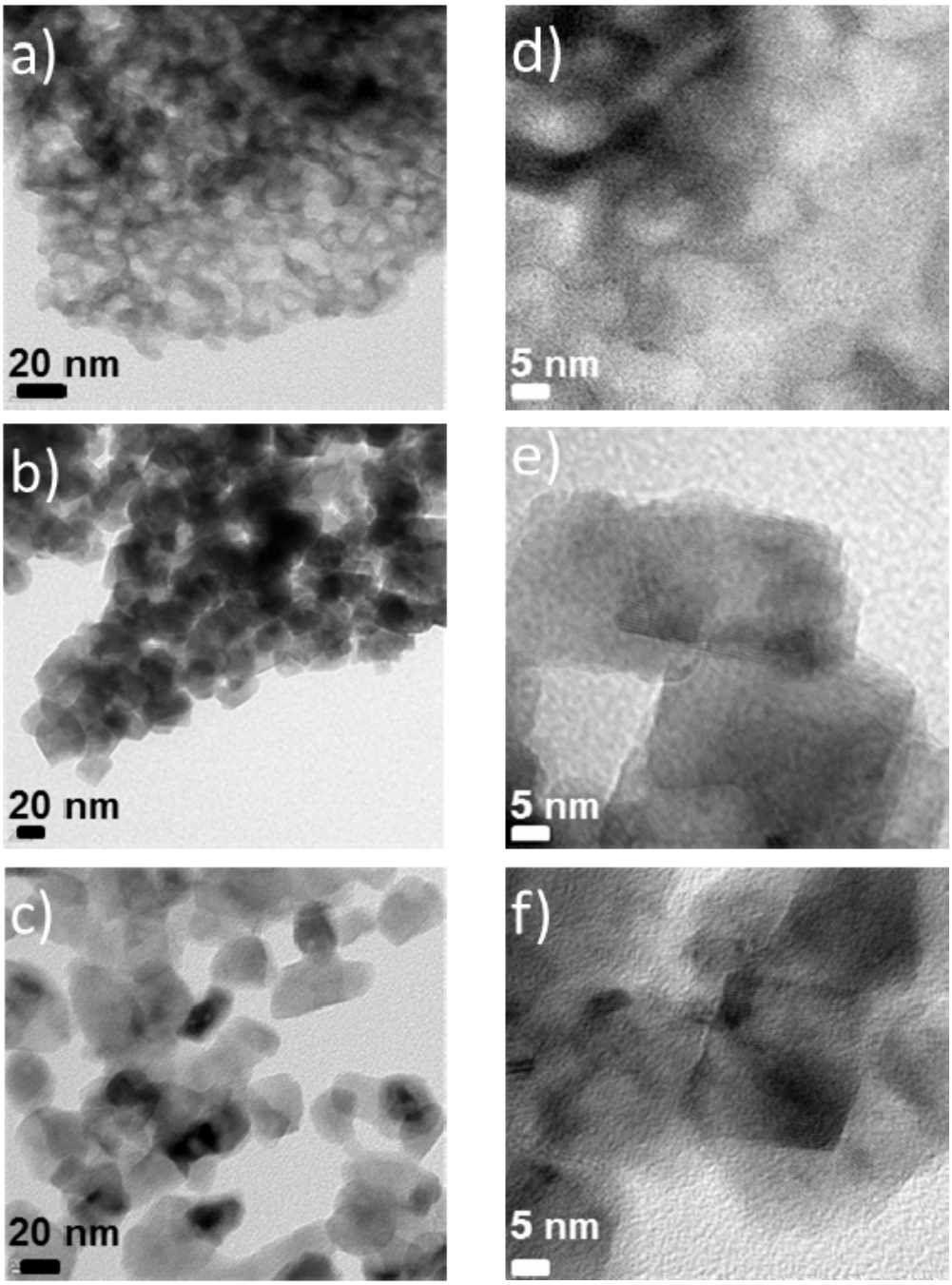

Figure S6. TEM images of a) $CaMn_2O_x$-0.8-550, b) $CaMn_2O_x$-4-550, c) $CaMn_2O_x$-8-550 and (HR)TEM images of d) $CaMn_2O_x$-0.8-550, e) $CaMn_2O_x$-4-550, f) $CaMn_2O_x$-8-550.

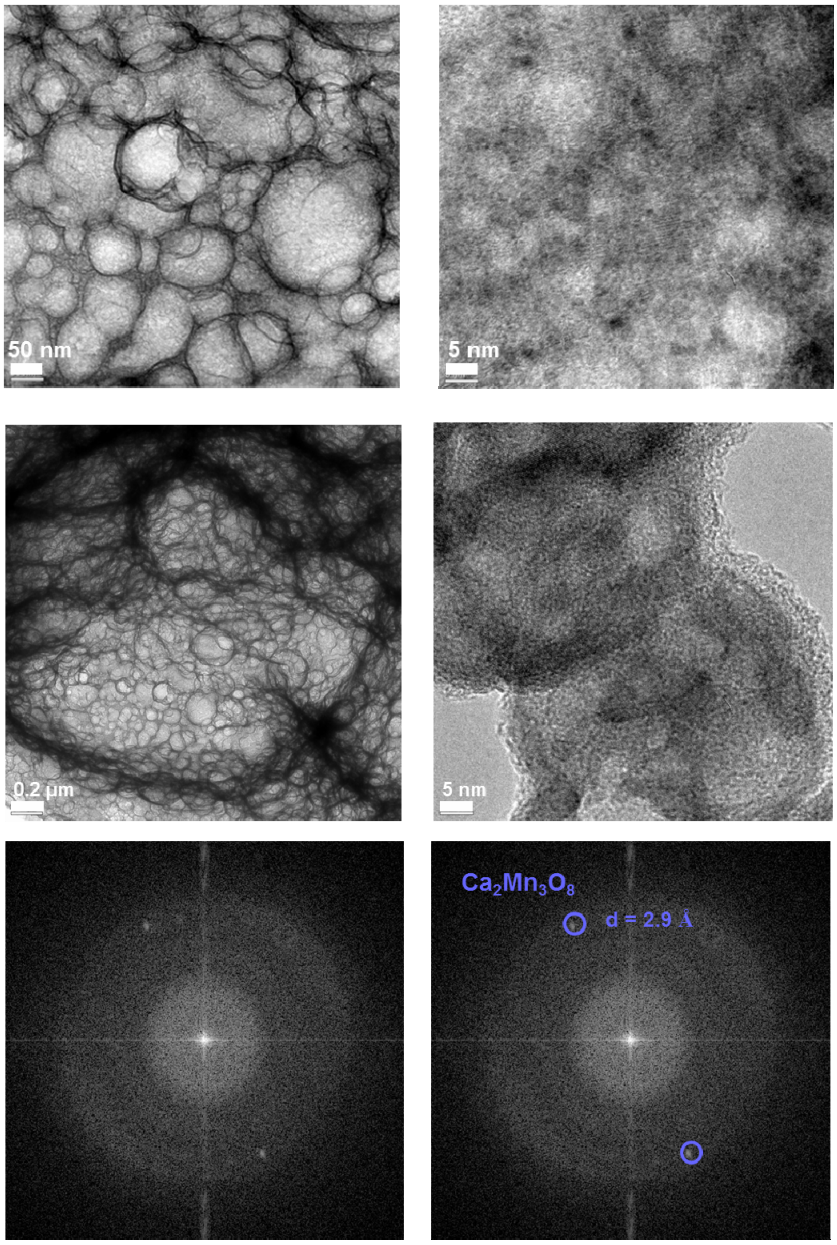

Figure S7. (HR)TEM images and FFTs of $CaMn_2O_x$-0.8-400 which shows d-values corresponding to $Ca_2Mn_3O_8$ (hkl=-311).

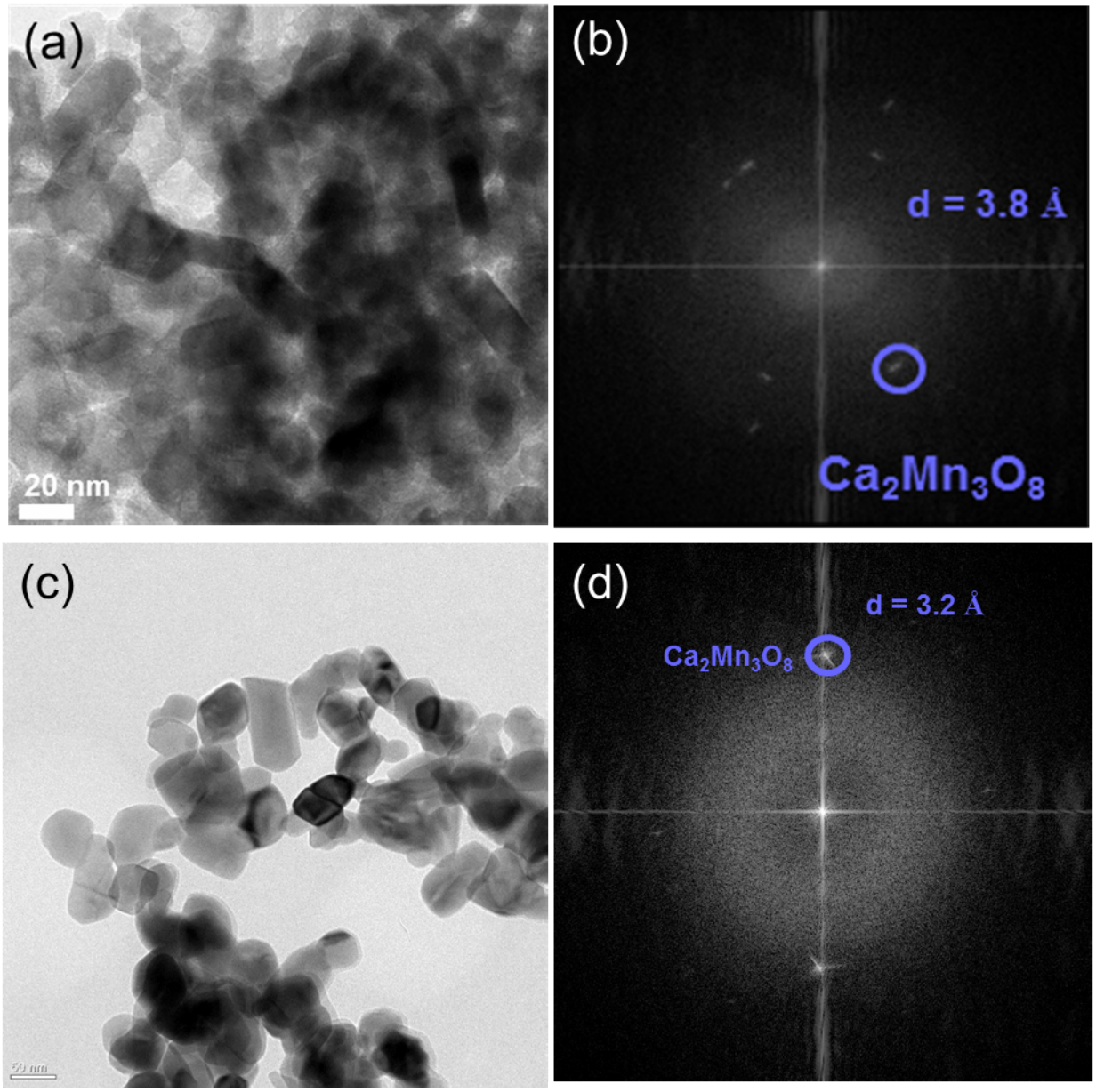

Figure S8. TEM images and FFTs of a,b) $CaMn_2O_x$-0.8-550 which shows d-values corresponding to $Ca_2Mn_3O_8$ (hkl=-111) and c,d) $CaMn_2O_x$-0.8-700 with d-values corresponding to $Ca_2Mn_3O_8$ (hkl=111).

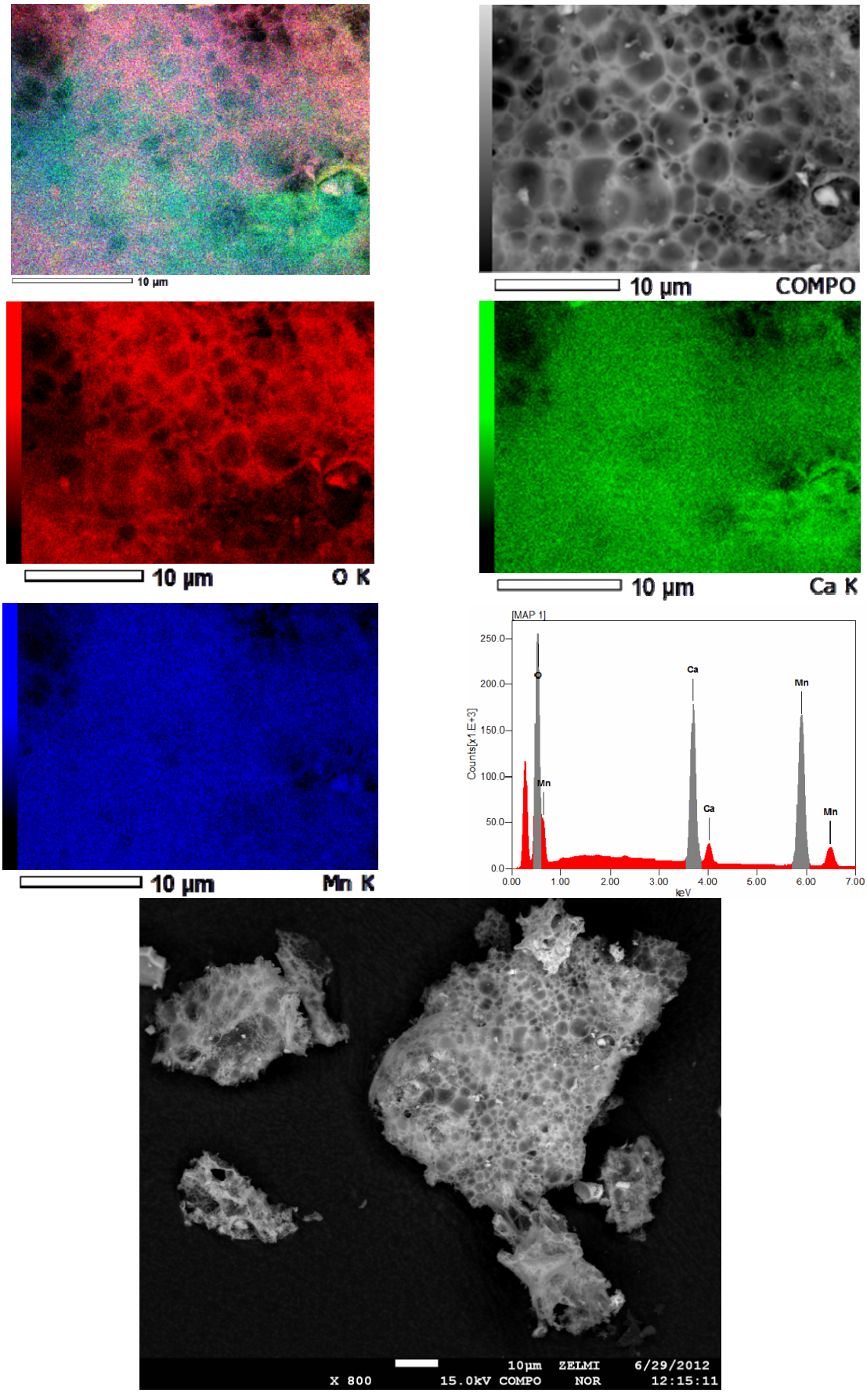

Figure S9. SEM image and EDS-mapping of $CaMn_2O_x$-0.8-400.

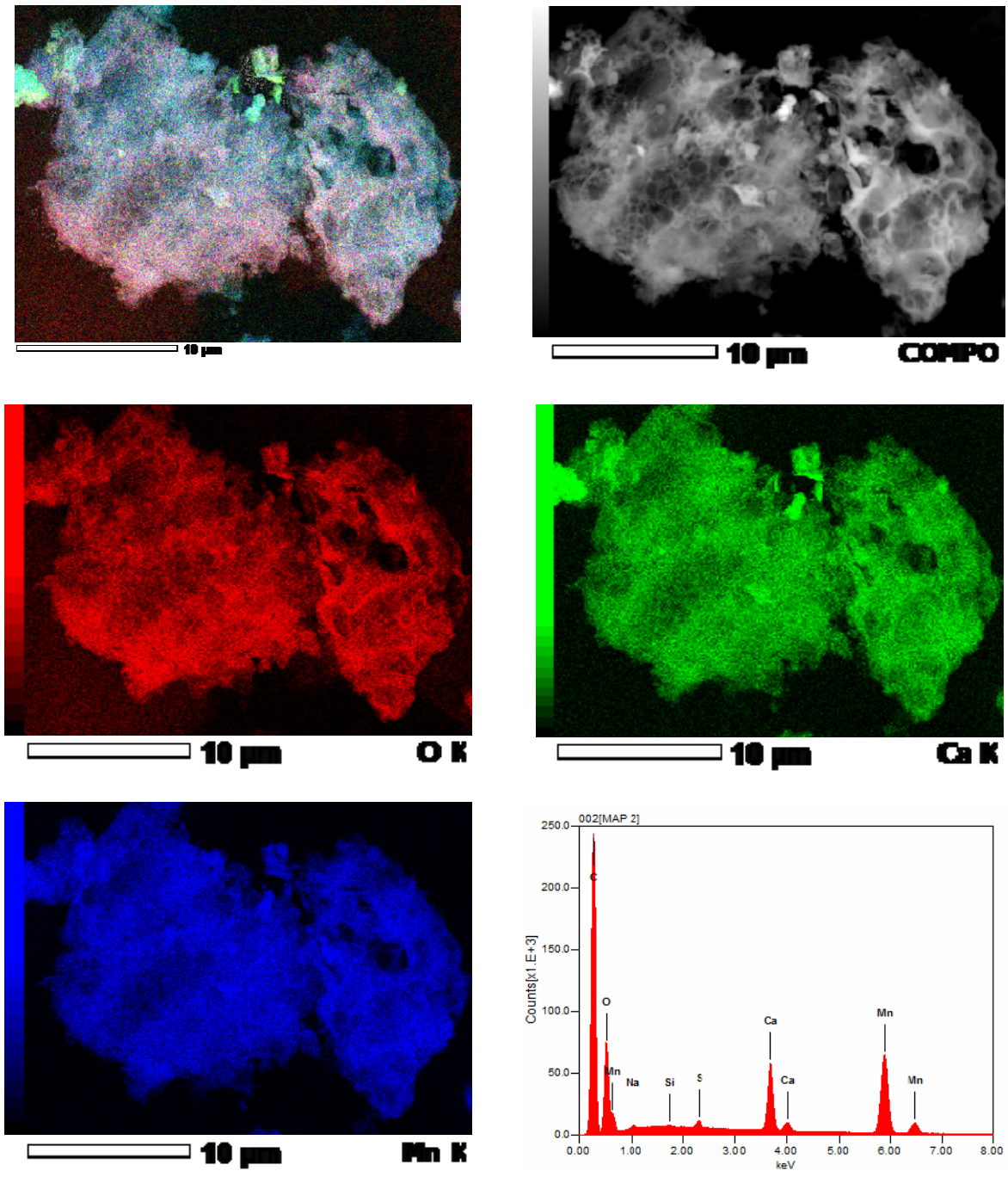

Figure S10. SEM image and EDS-mapping images of o $CaMn_2O_x$-0.8-550.

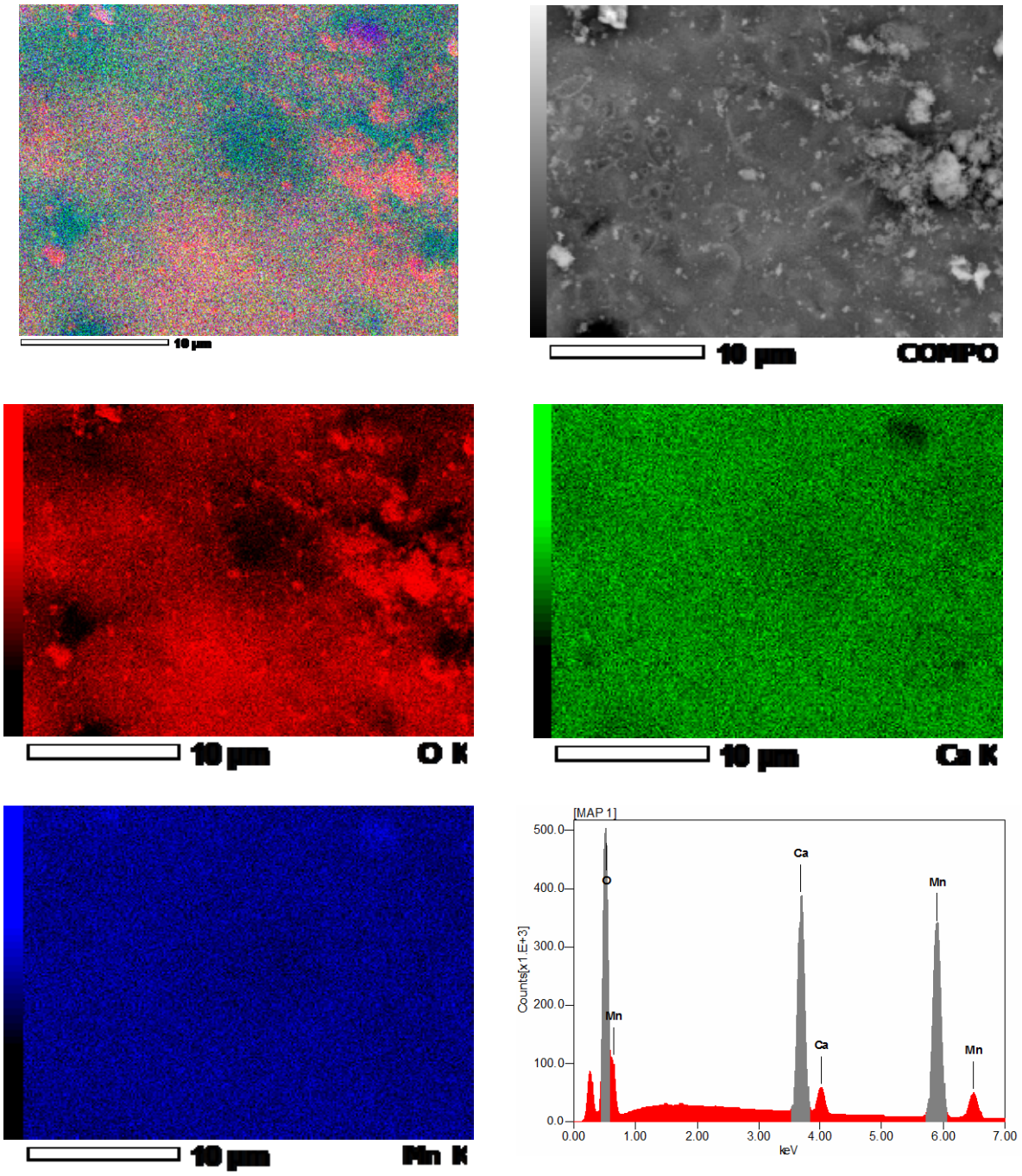

Figure S11. SEM image and EDS-mapping images of $CaMn_2O_x$-0.8-700.

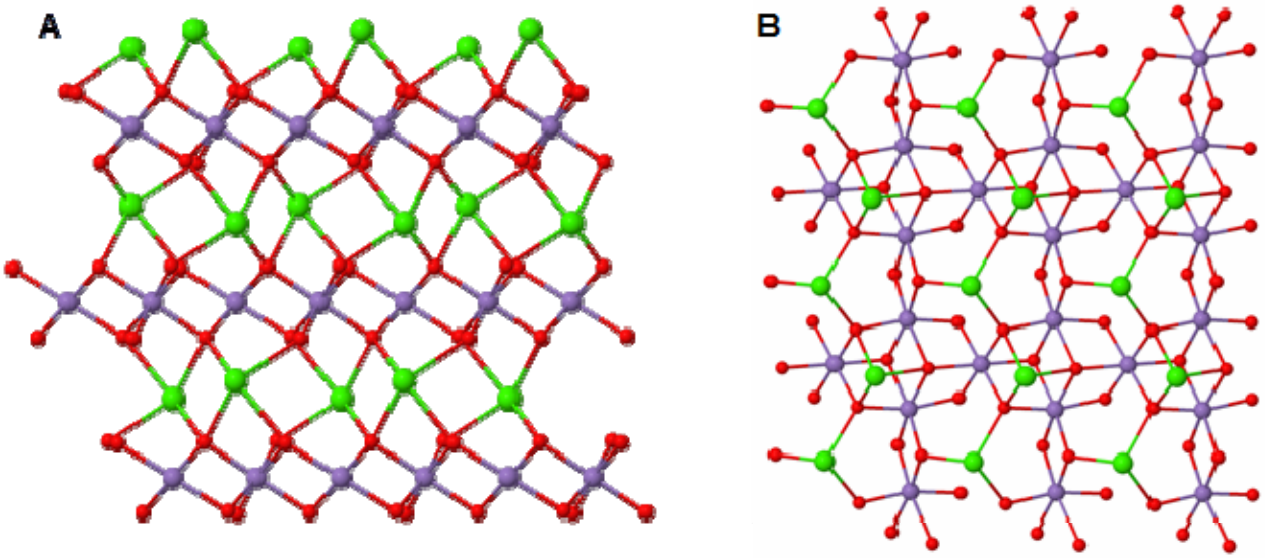

Figure S12. Structure of $Ca_2Mn_3O_8$. A – side view in which the MnO_6 layers of edge-sharing octahedral and the Ca ions connecting MnO_6 layers are visible. B – top view illustrating the two binding positions of Ca: (i) on the top of Mn vacancies (3.7 Å Mn-Ca distance) and in a cubane motif (3.3 Å Mn-Ca distance). Mn atoms are shown in magenta, Ca in green, and O in red.

Table S3. Oxygen evolution data from refs.[2,3] and as determined in the present investigation.

Sample	Rate (mmol O_2.mol Mn^{-1}. s^{-1})
$CaMn_2O_x$-8-550	0,14
$CaMn_2O_x$-4-550	0,219
$CaMn_2O_x$-0.8-550	0,62
$CaMn_2O_x$-0-550	0,029
$CaMn_2O_x$-0.8-300	0,011
$CaMn_2O_x$-0.8-400	3
$CaMn_2O_x$-0.8-700	0,082
$CaMn_2O_x$-0.8-100	0,018
Mn_2O_3-0.8-550	0,101
α-Mn_2O_3 [1]	0,027
$CaMn_2O_4.4H_2O$(2)[1]	0,325
$CaMn_2O_4.H_2O$(3)[1]	0,54
$CaMn_2O_4.4H_2O$(5)[1]	0,29
$Ca_{0.14}$-birnessite[2]	0,311
$Ca_{0.27}$- birnessite [2]	0,239

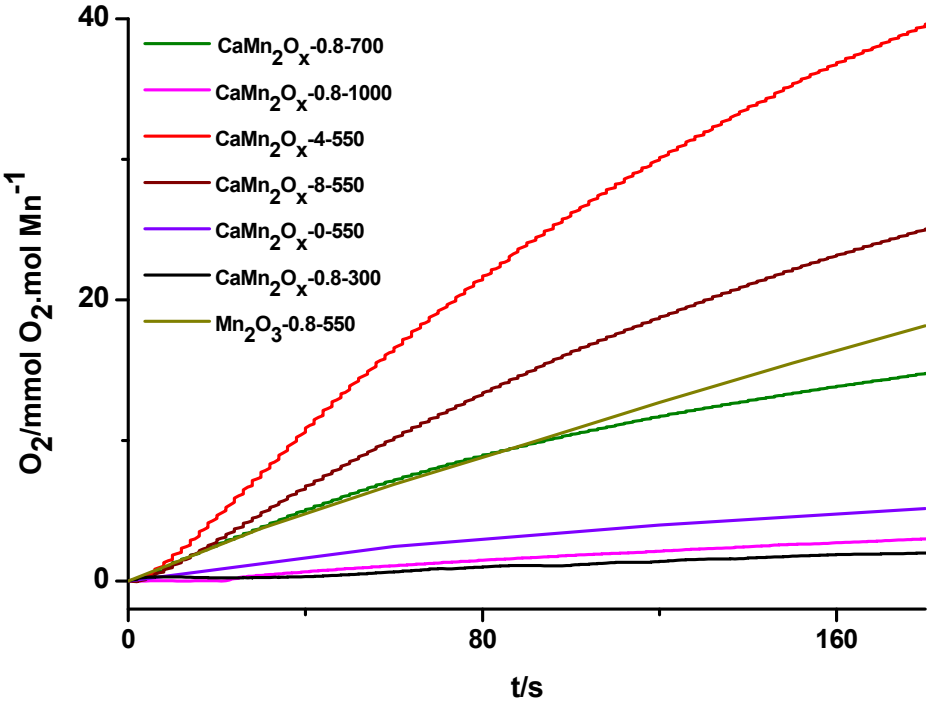

Figure S13. Oxygen evolution results for the reaction of CaMn oxides suspended in 0.5 M aqueous solution of Ce^{4+}.

Table S4: Amount of dissolved oxides (mg/ml) in solution (0.5M Ce(IV)).

Sample	Oxide amount(mg/ml)
$CaMn_2O_x$-0.8-300	0.5
$CaMn_2O_x$-0.8-400	0.05
$CaMn_2O_x$-0.8-550	0.5
$CaMn_2O_x$-0.8-700	0.5
$CaMn_2O_x$-0.8-1000	0.5
$CaMn_2O_x$-8-550	0.5
$CaMn_2O_x$-4-550	0.5
$CaMn_2O_x$-0-550	0.5
Mn_2O_3-0.8-550	0.45

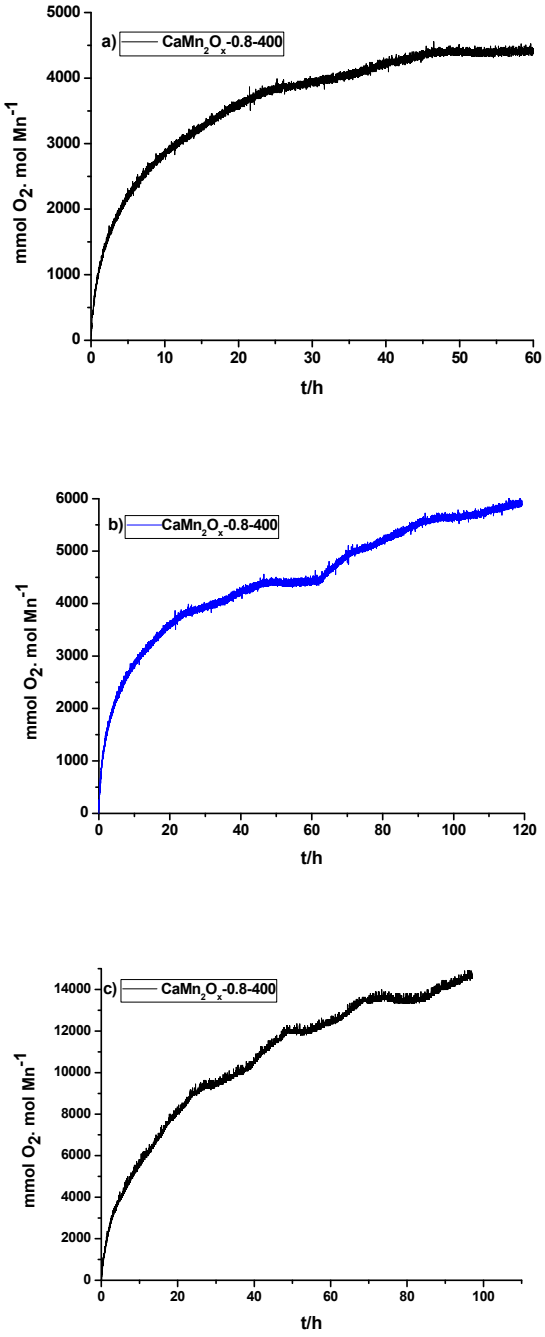

Figure S14: a) Long-term oxygen evolution test (100 mg catalyst in 38 ml of 0.5M Ce(IV) solution) by gas chromatography. The oxygen evolution rate is continuously decreasing likely because the oxidant, Ce(IV), is consumed. Nonetheless, oxygen evolution is detectable for more than two days. b) Regaining the activity after injection of 12 ml fresh Ce(IV) solution. Slower rate observed due to lower concentration of Ce(IV) in solution (0.12 M) after injection. c) Catalytic activity test with less amount of catalyst (20 mg in 38 ml of 0.5 M Ce(IV) solution.)

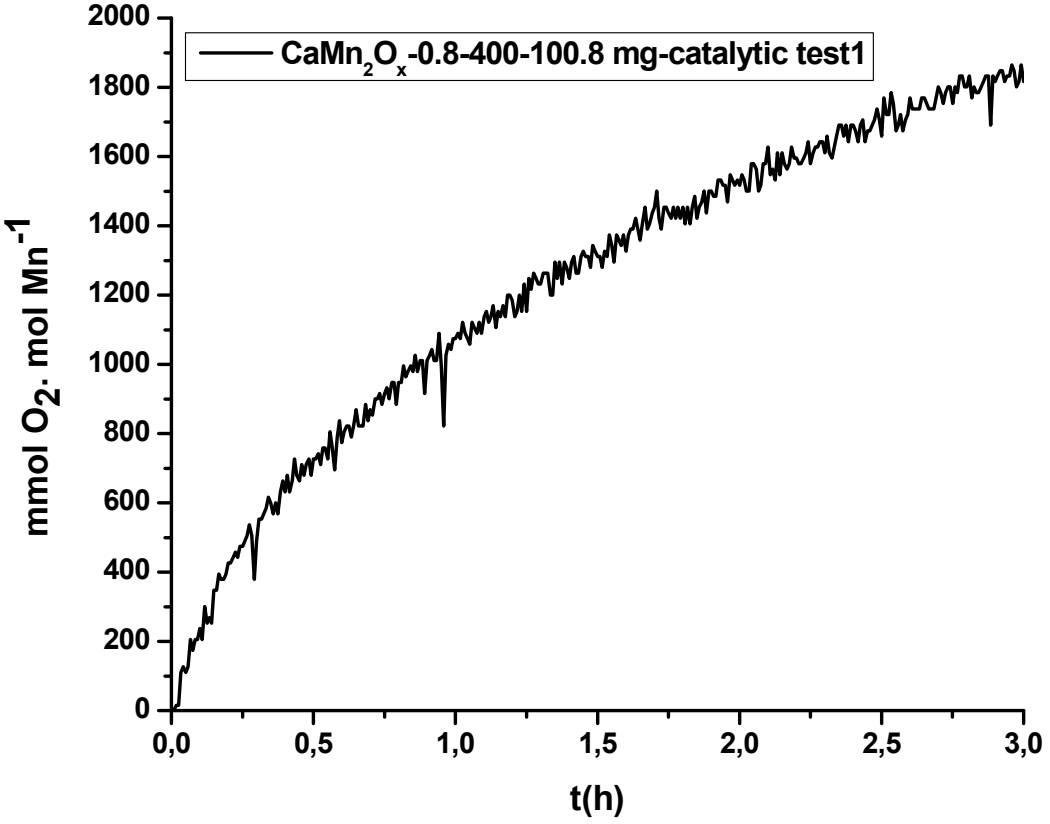
CaMn2Ox-0.8-400-100.8 mg-catalytic test1
mmol O2. mol Mn-1
t(h)
0
200
400
600
800
1000
1200
1400
1600
1800
2000
0,0
0,5
1,0
1,5
2,0
2,5
3,0

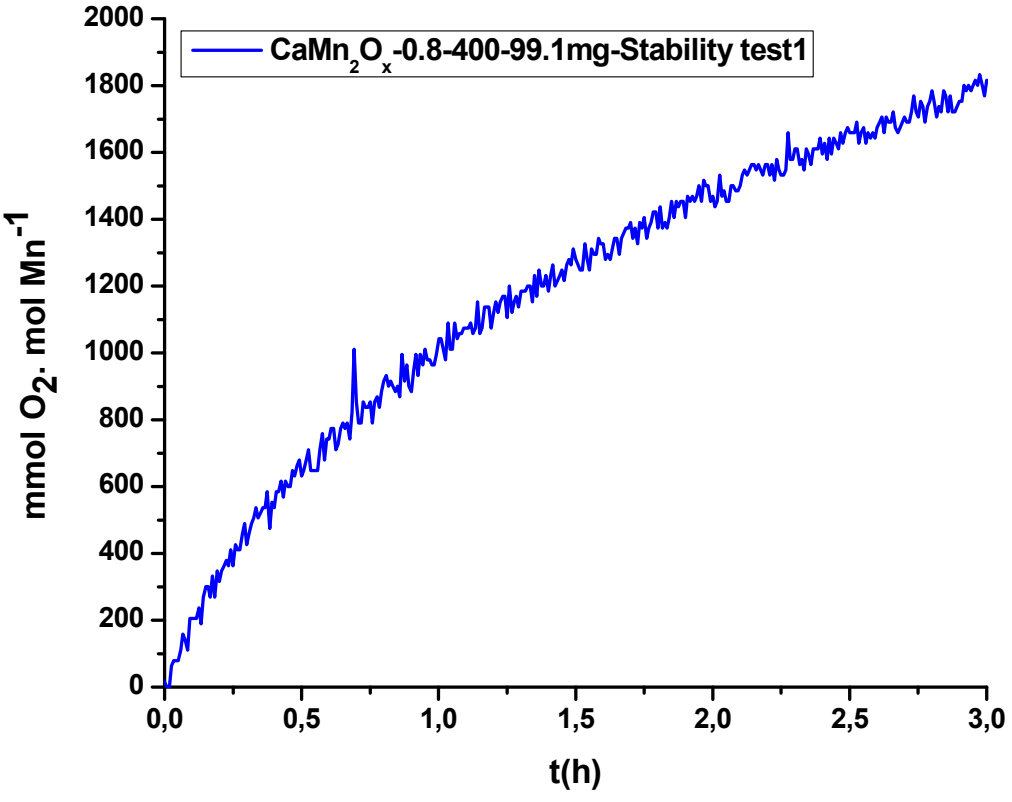
CaMn2Ox-0.8-400-99.1mg-Stability test1
mmol O2. mol Mn-1
t(h)
0
200
400
600
800
1000
1200
1400
1600
1800
2000
0,0
0,5
1,0
1,5
2,0
2,5
3,0

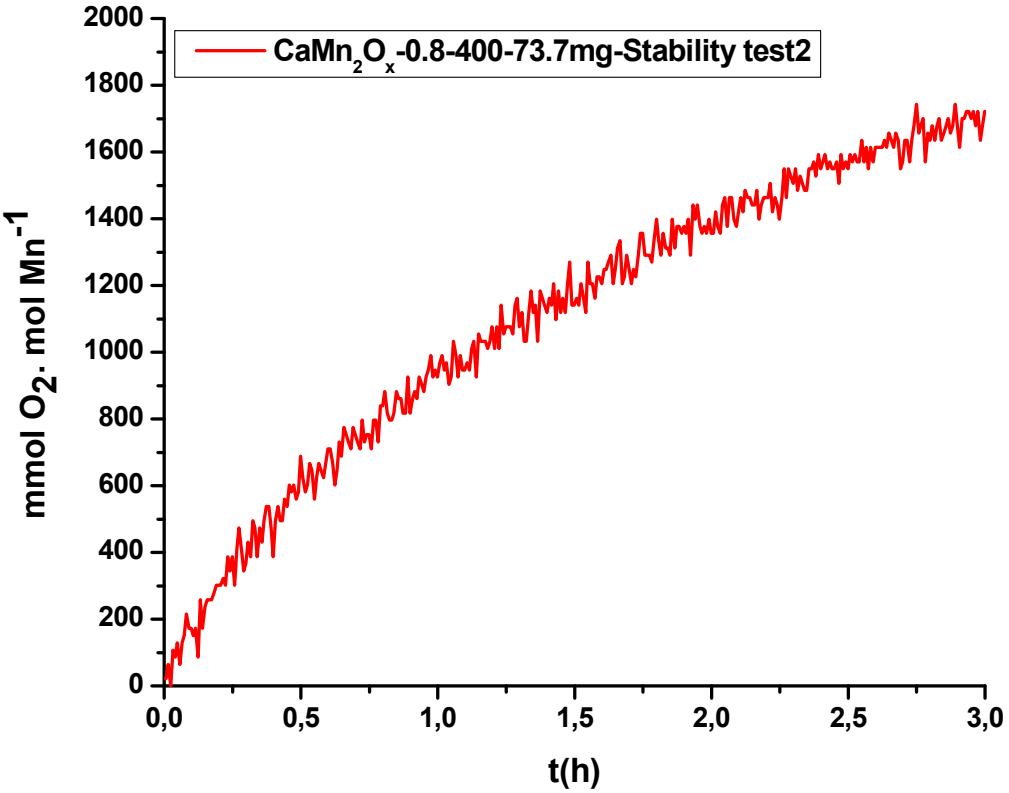

Figure S15: Recycling experiments using $CaMn_2O_x$-0.8-400; Black) first run, blue) second and red) third run. After each run the catalyst was recovered by filtration, washed several times with water, dried and then used again.

Table S5: Catalytic test results from gas chromatography (in 0.5 M Ce(IV)) for repeated addition of Ce(IV) (0.5 M Ce(IV) per run.

The TOF has been calculated based on the oxygen amount (in mmol) produced in the first 30 min of the reaction and divided by the amount of manganese of the catalyst (in mol).

Test	T (^oC)	Cat amount (mg)	TOF ($mmolO_2.molMn.s^{-1}$)
Long-term	23	100.8	0.42
Run 1	24.2	100.8	0.40
Run2	25	99.1	0.35
Run3	25	73.7	0.35

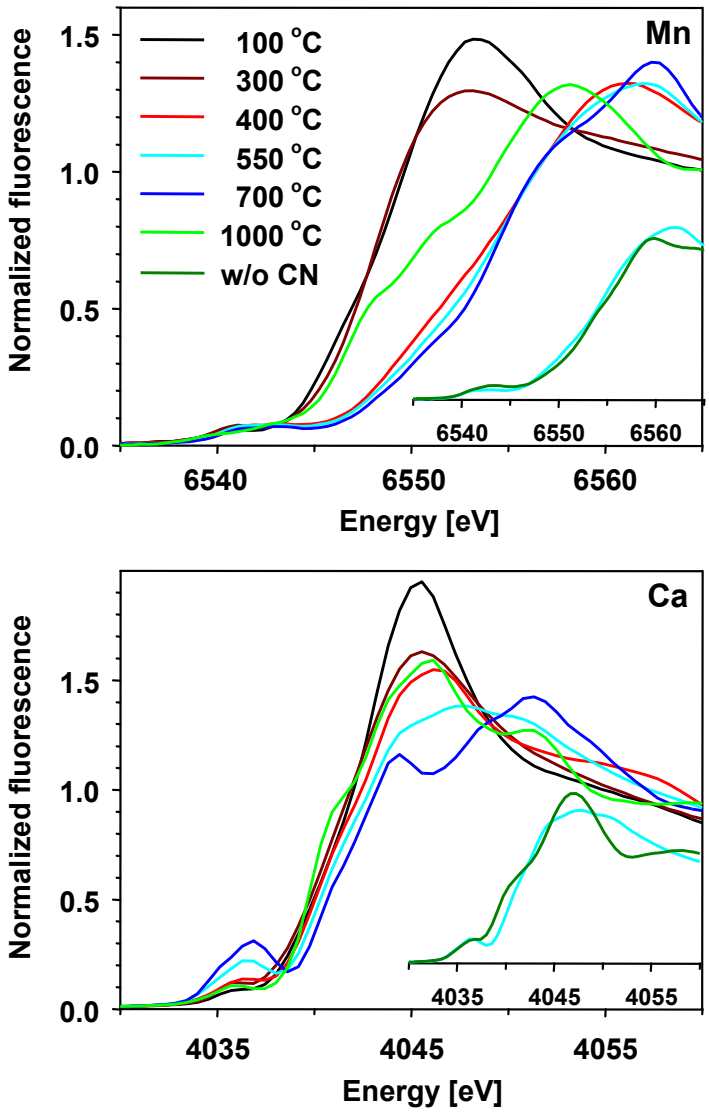

Figure S16. XANES spectra measured at the Mn *K*-edge (top) and the Ca *K*-edge (bottom) from the CaMn material before annealing (labeled '100 °C') and after annealing for 4 h at the indicated temperature. Insets: comparison of the XANES spectra from CaMn oxide with and without cyanamide, annealed at 550 °C.

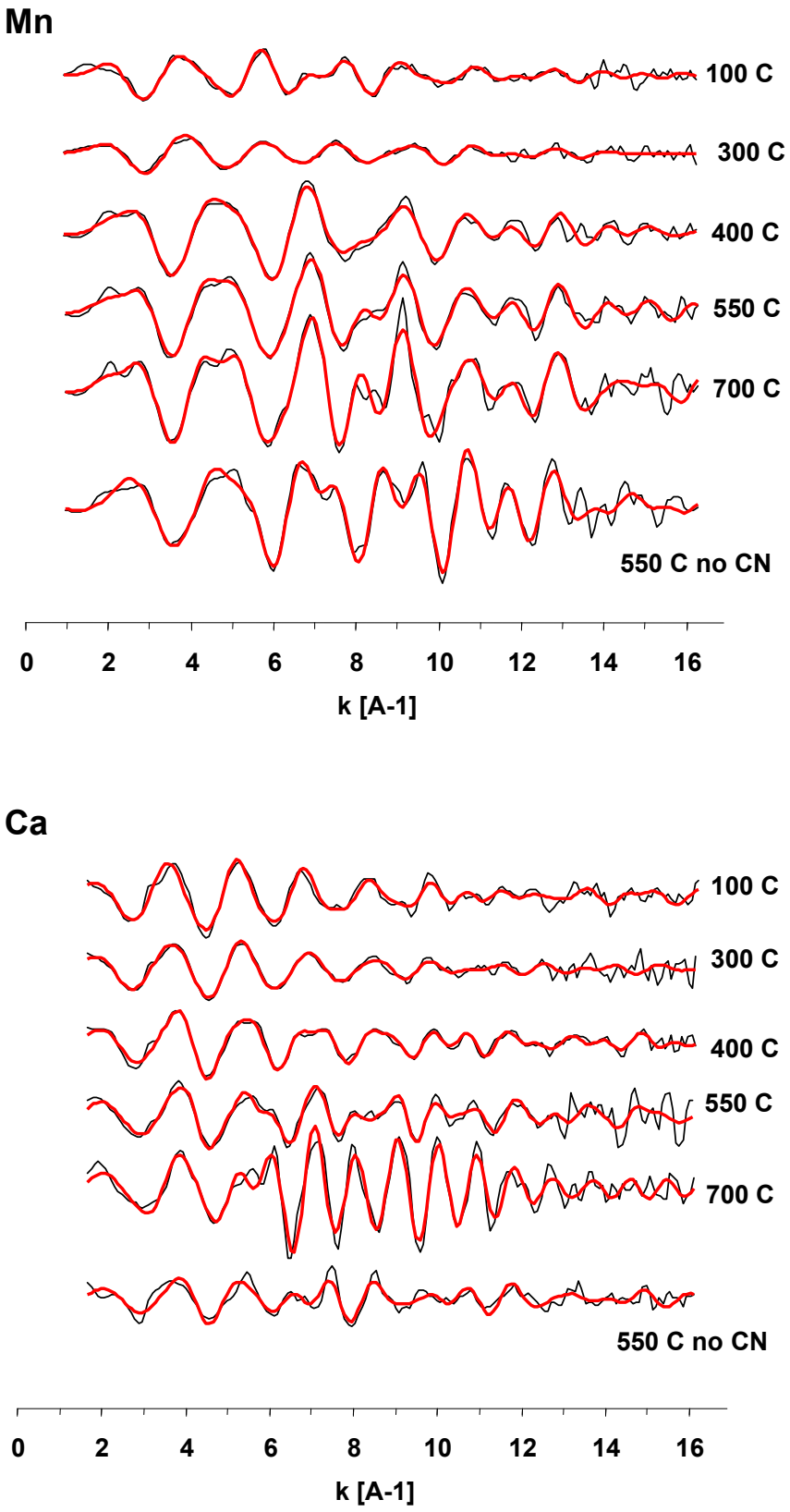

Figure S17. k^3-weighted EXAFS spectra measured at the Mn *K*-edge (top) and the Ca *K*-edge (bottom) from the CaMn material before annealing (labeld '100 °C') and after annealing for 4 h at the indicated temperature. Black: experimental curves, red - simulations. The simulation parameters are shown in Table S1.

Table S6. EXAFS simulation parameters and 1σ uncertainty ranges in the EXAFS fit parameters. Parameters marked by * were constrained. All Mn-Ca distances were constrained to be equal in the Mn and Ca spectra, e.g., equal Mn-Ca distances in the Mn-EXAFS and the Ca-EXAFS (joint-fit approach). For simulation of the first manganese coordination sphere, two shells of backscattering atoms were used and the sum of the two coordination numbers was constrained to be equal to six. In the two-shell simulation of the first Ca and Mn coordination sphere, the values of the Debye-Waller parameter (denoted as σ or s) were constrained to be equal.

	N		R, A		s, A		N		R, A		s, A	
	Mn-O						Ca-O					
100 oC	0.9 ±	0.2	1.91 ±	0.026	0.09 ±	0.005	3.4 ±	0.2	2.36 ±	0.006	0.05 ±	0.005
300 oC	1.4 ±	0.1	1.90 ±	0.009	0.09 ±	0.003	2.0 ±	0.2	2.30 ±	0.011	0.07 ±	0.007
400 oC	5.5 ±	0.1	1.88 ±	0.00	0.08 ±	0.00	3.7 ±	0.4	2.35 ±	0.01	0.06 ±	0.01
550 oC	5.4 ±	0.2	1.89 ±	0.00	0.07 ±	0.00	3.4 ±	0.3	2.33 ±	0.01	0.05 ±	0.01
700 oC	5.5 ±	0.2	1.89 ±	0.00	0.06 ±	0.00	3.0 ±	1.1	2.28 ±	0.03	0.08 ±	0.02
550 oC no CN	5.2 ±	0.2	1.89 ±	0.00	0.06 ±	0.00	2.6 ±	0.3	2.37 ±	0.01	0.0632* ±	0.00
	Mn-O						Ca-O					
100 oC	5.14* ±	0.0	2.17 ±	0.01	0.0911* ±	0.00	3.8 ±	0.3	2.50 ±	0.006	0.0541* ±	0.00
300 oC	4.61* ±	0.0	2.15 ±	0.01	0.0933* ±	0.00	3.9 ±	0.4	2.44 ±	0.01	0.0698* ±	0.00
400 oC	0.52* ±	0.0	2.29 ±	0.04	0.0797* ±	0.00	2.1 ±	0.2	2.48 ±	0.01	0.0622* ±	0.00
550 oC	0.641* ±	0.0	2.29 ±	0.03	0.0732* ±	0.00	1.8 ±	0.2	2.48 ±	0.01	0.0548* ±	0.00
700 oC	0.529* ±	0.0	2.31 ±	0.04	0.0605* ±	0.00	3.0 ±	1.0	2.39 ±	0.03	0.0818* ±	0.00
550 oC no CN	0.849* ±	0.0	2.21 ±	0.02	0.0624* ±	0.00	1.4 ±	0.3	2.55 ±	0.02	0.0632* ±	0.00
	Mn-Mn						Ca-Ca					
100 oC	0.3 ±	0.1	2.90 ±	0.026	0.0632* ±	0.00	1.3 ±	0.3	4.41 ±	0.013	0.0632* ±	0.00
300 oC	0.2 ±	0.1	2.87 ±	0.02	0.0632* ±	0.00	0.8 ±	0.6	3.61 ±	0.08	0.0632* ±	0.00
400 oC	1.5 ±	0.1	2.87 ±	0.00	0.0632* ±	0.00	2.4 ±	0.3	4.08 ±	0.01	0.0632* ±	0.00
550 oC	1.8 ±	0.1	2.87 ±	0.00	0.0632* ±	0.00	1.1 ±	0.4	4.76 ±	0.02	0.0632* ±	0.00
700 oC	2.7 ±	0.3	2.88 ±	0.00	0.0620 ±	0.00	2.9 ±	0.6	3.46 ±	0.01	0.0632* ±	0.00
550 oC no CN	1.3 ±	0.2	2.87 ±	0.01	0.0632* ±	0.00	1.3 ±	0.3	4.07 ±	0.02	0.0632* ±	0.00
	Mn-O/C/Mn						Ca-O/C					
100 oC	3.9 ±	1.0	3.22 ±	0.03	0.0632* ±	0.00	3.1 ±	1.1	3.73 ±	0.02	0.0632* ±	0.00
300 oC	1.9 ±	0.4	3.11 ±	0.02	0.0632* ±	0.00	5.2 ±	1.2	3.73 ±	0.03	0.0632* ±	0.00
400 oC	3.4 ±	1.0	3.52 ±	0.02	0.0632* ±	0.00	1.4 ±	0.7	3.66 ±	0.03	0.0387* ±	0.00
550 oC	6.8 ±	2.3	3.487* ±	0.00	0.0387* ±	0.00	3.37 ±	0.9	3.707 ±	0.044	0.0632* ±	0.00
700 oC	6.0 ±	0.0	3.58 ±	0.01	0.0632* ±	0.00	4.6 ±	1.6	3.69 ±	0.05	0.0632* ±	0.00
550 oC no CN	3.9 ±	0.3	3.43 ±	0.00	0.0632* ±	0.00						
	Mn-Ca						Ca-Mn					
400 oC	0.2 ±	0.2	3.17 ±	0.01	0.0632* ±	0.00	0.4 ±	0.1	3.166* ±	0.00	0.0632* ±	0.00
550 oC	2.8 ±	0.8	3.24 ±	0.01	0.0632* ±	0.00	0.3 ±	0.2	3.239* ±	0.00	0.0632* ±	0.00
700 oC	0.2 ±	0.3	3.31 ±	0.01	0.0632* ±	0.00	1.6 ±	0.4	3.313* ±	0.00	0.0632* ±	0.00
550 oC no CN	2.6 ±	0.3	3.18 ±	0.01	0.0632* ±	0.00	1.1 ±	0.2	3.18* ±	0.00	0.0632* ±	0.00
	Mn-Mn						Ca-Ca					
100 oC	1.4 ±	0.3	3.35 ±	0.01	0.0632* ±	0.00	0.6 ±	0.2	3.549 ±	0.02	0.0632* ±	0.00
300 oC	0.3 ±	0.1	3.38 ±	0.02	0.0632* ±	0.00	0.3 ±	0.6	3.50 ±	0.13	0.0632* ±	0.00
400 oC	1.0 ±	0.3	3.38 ±	0.01	0.0632* ±	0.00	0.4 ±	0.3	3.53 ±	0.03	0.0632* ±	0.00
550 oC	4.0 ±	1.4	3.36 ±	0.01	0.0632* ±	0.00	1.2 ±	0.3	3.46 ±	0.01	0.0632* ±	0.00
	Mn-Ca						Ca-Mn					
400 oC	0.0 ±	0.2	3.84 ±	0.01	0.0632* ±	0.00	1.0 ±	0.3	3.84* ±	0.00	0.0632* ±	0.00
550 oC	2.0 ±	0.5	3.68 ±	0.01	0.0632* ±	0.00	0.8 ±	0.7	3.679* ±	0.00	0.0632* ±	0.00
700 oC	2.0 ±	0.4	3.70 ±	0.02	0.0632* ±	0.00	3.4 ±	0.7	3.701* ±	0.00	0.0632* ±	0.00
							Ca-Ca					
400 oC							0.2 ±	0.7	4.45 ±	0.07	0.0632* ±	0.00
550 oC							1.8 ±	0.9	5.42 ±	0.02	0.0632* ±	0.00
700 oC							2.3 ±	0.4	4.34 ±	0.01	0.0632* ±	0.00
550 oC no CN							0.2 ±	0.4	4.48 ±	0.12	0.0632* ±	0.00

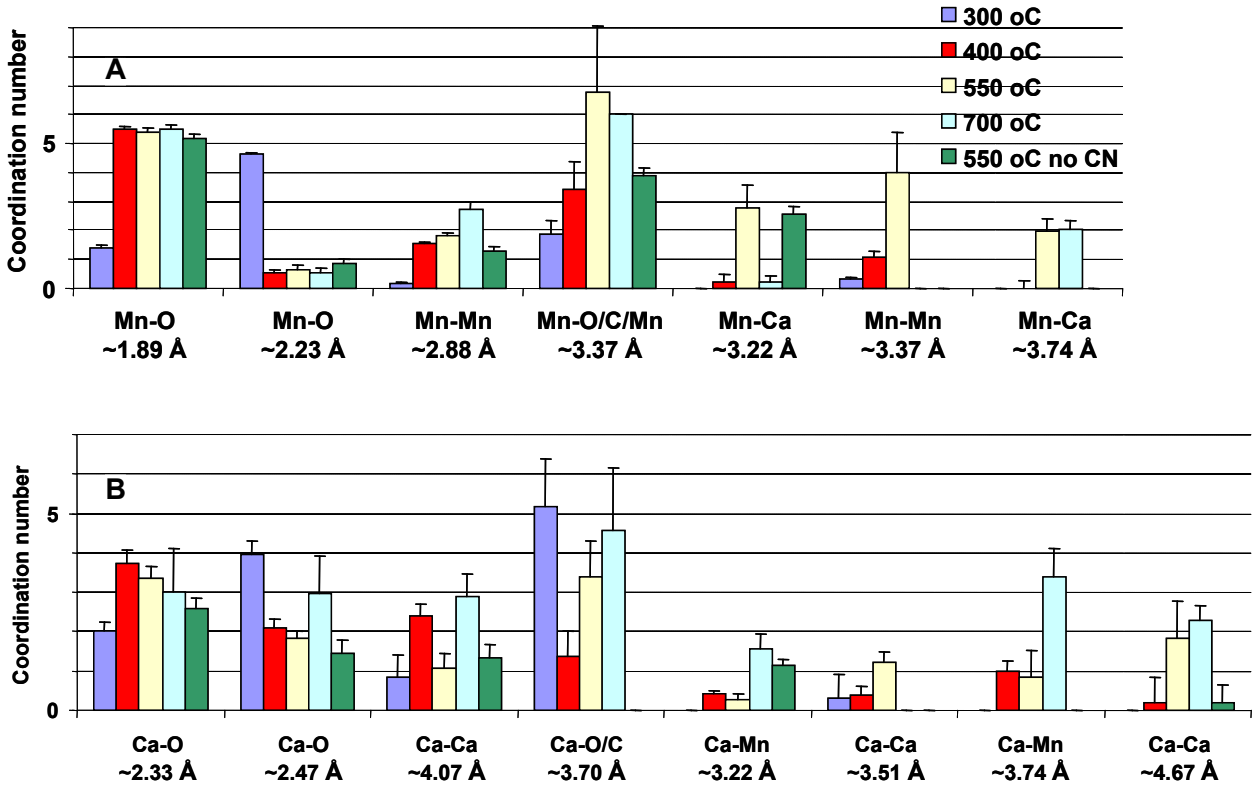

Figure S18. Graphical presentation of the coordination numbers from Table S5. A, measurements at the Mn *K*-edge; B, at the Ca *K*-edge.

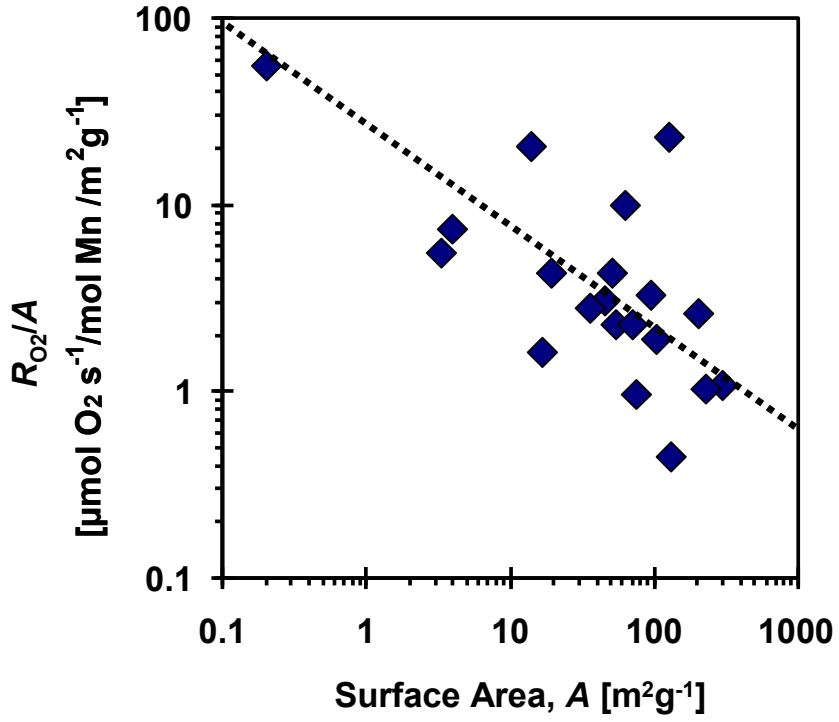

Figure S19. Rate of O_2-formation (R_{O2}) per surface area (A) derived from the values in Table S1. If O_2-rate were proportional to the surface area, R_{O2}/A should be independent on the surface (A). Instead, a decreased activity per surface area by two orders of magnitude is observed meaning that the surface area is not the decisive determinant of the rate of catalysis (see dotted line drawn to guide the eye) (refs.[1,2] and this investigation).

References:

[1] M. Schwarze, D. Stellmach, M. Schröder, K. Kailasam, R. Reske, A. Thomas, R. Schomäcker, Phys. Chem. Chem. Phys., 2013, 15, 3466-3472.

[2] M. M. Najafpour, T. Ehrenberg, M. Wiechen and P. Kurz, Angew. Chem., Int. Ed. , 2010, 49, 2233-2237.

[3]M. Wiechen, I. Zaharieva, H. Dau and P. Kurz, Chemical Science, 2012, 3, 2330-2339.